Optimization of a search for doubly-charged Higgs bosons in same-sign di-muon final states at $\sqrt{s} = 8\,\text{TeV}$ with the ATLAS detector

Master's Thesis by Leonora Vesterbacka Olsson

Supervised by Else Lytken
30 ECTS over the academic year 2014-2015
Department of Particle Physics
Lund University
Sweden

LUND
UNIVERSITY

Contents

Introduction

In this thesis an optimization of a previously performed inclusive search for beyond Standard Model Physics in same-sign di-lepton final states is performed, but tuned for a doubly-charged Higgs boson decaying to same-sign di-muons. The doubly-charged Higgs boson is a proposed fundamental particle whose existence would provide evidence for theoretical extensions of the Standard Model (SM) of particle physics. The aim of the optimization is to see whether one can improve on the sensitivity on the mass limits set by previously performed searches for doubly-charged Higgs bosons with the ATLAS detector at the Large Hadron Collider (LHC) at CERN. Assuming a branching of 100 % for a decay into two leptons with the same charge provides a clean signal that can be distinguished from ordinary SM background processes. I examine different variables such as leading muon transverse momentum p_{T} and azimuthal angular difference $\Delta\phi$ and invariant mass of the muon pair, where the signal and background yields differ and make a selection (a cut) on these variables. The aim of the selection is to reduce the SM background while keeping the signal i.e. to maximize the significance. The analysis is done using $20.3\,\mathrm{fb}^{-1}$ of proton-proton collisions recorded at a center of mass energy of $\sqrt{s}$ =8 TeV with the ATLAS detector at the LHC in 2012. Five different signal regions are examined, corresponding to mass points of $m_{H^{\pm\pm}} = 150\,\mathrm{GeV}$, $m_{H^{\pm\pm}} = 300\,\mathrm{GeV}$, $m_{H^{\pm\pm}} = 500\,\mathrm{GeV}$, $m_{H^{\pm\pm}} = 600\,\mathrm{GeV}$ and $m_{H^{\pm\pm}} = 1000\,\mathrm{GeV}$. The thesis is structured as follows. The first section consists of a brief introduction to the world of particle physics and a description of the Standard Model and the Standard Model Lagrangian. The subsequent section contains a description of the LHC and the ATLAS detector. The analysis is thereafter presented along with a description of the two types of SM backgrounds, the prompt and non-prompt backgrounds, the event selection and the optimization procedure. The results contain a presentation of the selected cuts, their efficiency, the obtained significances and the results when applying the cuts to real data. Finally, the necessity of the cuts is evaluated by comparing the obtained significances in the different cases where all, some or none of the cuts were applied.

1 Theory

The Standard Model has since the 1960s been the most successful theory describing the smallest constituents of matter, the elementary particles. Its' success is due to the many theoretical predictions that have been experimentally tested at high energy physics laboratories such as CERN. The model establishes a set of fundamental particles that can be divided into fermions and bosons depending on their spin. The fermions, possessing half-integer spin, can further be divided into quarks and leptons. These are the building blocks of matter. The other fundamental particles of the SM, the gauge bosons, are force mediators that carry the fundamental forces such as the electromagnetic, strong and weak forces.

The most recent success of the Standard Model was the discovery of the Higgs boson in 2012. The Higgs is a particle introduced to explain how some particles gain mass and whose existence was predicted in the 1960s. Although the SM has proven successful in theoretically predicting the existence of particles that have later been experimentally discovered at high energy physics laboratories, it is still not a complete theory. For example, it only manages to describe three out of four fundamental forces, and is unable to describe phenomena such as dark matter. Therefore, theorists and experimentalists are led to believe that extensions of the SM must exist to account for the unanswered questions in the universe. Some of these extended SM theories are studied in this thesis, namely the theories that predict a doubly-charged Higgs boson. But before these theories are introduced, I will give a brief introduction to the formulation of the SM using the SM Lagrangian, and a presentation of the Higgs boson.

1.1 The Standard Model Lagrangian

The Standard Model is a relativistic quantum field theory, which means that the particles we know are described as excitations of fields in space-time. The idea is to describe the theory using the SM Lagrangian $\mathcal{L}$, which is a quantity containing all the dynamics of the theory, i.e. it explains all the interactions between all the particles in one equation. I will proceed by using the conventions and notations found in [1] and ask the reader for patience regarding technical terms and the far from complete description of the SM Lagrangian. From a classical point of view, the Lagrangian is just defined as the kinetic energy minus the potential energy, $\mathcal{L} = T - V$. From a group theory point of view, the SM Lagrangian is formulated using the powerful tool of gauge symmetries. The concept of symmetries is commonly used in physics and states that if a system is invariant under some symmetry transformation, such as the rotation of a sphere that leaves it just as it was before, each of these invariances under internal symmetries leads to conservation laws. For example, the invariance under a so-called $U(1)$ symmetry leads to the conservation of electric charge of the theory. There are three fundamental internal symmetries that define the SM theory, i.e. invariance under these internal symmetries generates all of the known forces. The symmetries that make up the theory is the gauge group:

$$U(1)_Y \times SU(2)_L \times SU(3)_C \tag{1}$$

where each term represents one of the gauge symmetries that generate the fundamental interactions and the force carriers. The $SU(3)_C$[1] group represents the gauge symmetry of quantum chromo dynamics which generates the 8 gluons, the mediators of the so-called strong force. The $SU(2)_L \times U(1)_Y$[2] group represents the gauge symmetry of electroweak interactions, which generate 3 massive bosons (Z and $W^{\pm}$). These are the mediators of the electroweak force. As mentioned above, the electromagnetic force mediator, the photon, is generated by the $U(1)$ internal symmetry. These symmetry transformations give us a hint on how to organize the fermions in the SM, and how to explain the manner in which the different fermions interact with each other through the gauge bosons. The leptons and quarks can be represented in left-handed $SU(2)$ doublets:

$$L^i = \begin{pmatrix} \nu_l^i \\ l^i \end{pmatrix}_L , \quad Q^i_{L,\alpha} = \begin{pmatrix} u^i_\alpha \\ d^i_\alpha \end{pmatrix}_L \tag{2}$$

and right-handed singlets:

$$l^i_R , \quad d^i_{R,\alpha} , \quad u^i_{R,\alpha} \tag{3}$$

where $\nu^i = \{\nu^e, \nu^\mu, \nu^\tau\}$ and $l^i = \{e, \mu, \tau\}$ are the leptons of the three generations. Similarly there are three generations of up-like quarks $u^i = \{u, c, t\}$ (called up, charm and top) and down-like quarks $d^i = \{d, s, b\}$ (called down, strange and bottom). This $SU(2)$ representation tells us that the quarks and leptons can interact with each other through the exchange of an electroweak gauge boson (the generators of the electroweak theory), Z, W^- or W^+. The subscript α in the representation of the quarks is introduced because the quarks can be put into so-called color $SU(3)$ triplets, assigning the quarks a new property: color $\alpha = r, g, b$ (red, green and blue). The leptons are color singlets (that carry no color and therefore no subscript α), and thus do not interact with the color charge mediators, the gluons. The Lagrangian of the theory can be expressed as:

$$\mathcal{L}_{ferm} = \sum_f \bar{f} i \gamma^\mu \mathcal{D}_\mu f \tag{4}$$

where the sum is over the different fermions $f = L$, e_R, Q_L, u_R and d_R. The $\mathcal{D}_\mu$ is the covariant derivative that ensures invariance under each of the gauge symmetries.

$$\mathcal{D}_\mu = \partial_\mu - i g_1 \frac{Y}{2} B_\mu - i g_2 \frac{\tau^i}{2} W^i_\mu - i g_3 \frac{\lambda^a}{2} G^a_\mu \tag{5}$$

where Y is the generator of $U(1)$ transformations, τ^i, $i = 1, 2, 3$ are the $SU(2)_L$ generators, and λ^a, $a = 1, 2, ..., 8$ are the $SU(3)_C$ generators. The terms W^i and B are the gauge fields of the electroweak interaction, and G^a_μ are gluon fields i.e. the gauge fields of the strong interaction. The coupling constants

[1] The subscript C stands for color.

[2] The subscript L stands for left and the subscript R stands for right. These subscripts refer to the chirality, or handedness, of a particle. The chirality is a property of the SM which tells us whether a transformation is under a right-handed or left-handed representation of the Poincaré group. The meaning of chirality is not very intuitive, but effects of chirality are incorporated in the SM, which treats left-handed and right-handed particles differently.

g_1, g_2 and g_3 are a measure of how strong the interactions are. To summarize, the SM Lagrangian in Equation (4) contains all the fundamental particles of the SM, i.e. the six quarks, the six leptons and the 12 gauge bosons. The only missing piece of the theory is to explain how these particle gain mass, which will be done in Sec. 1.2 treating the Higgs mechanism.

1.2 The Higgs Mechanism

The SM would not be a complete theory if it was unable to explain how particles gain mass. Fortunately, it does, and I will try to, in all brevity, walk you through the concept of spontaneous symmetry breaking (SSB), the Higgs mechanism, and finally introduce the Higgs boson.

Spontaneous Symmetry Breaking

The basic idea behind SSB is that if a system is described by a certain Lagrangian which is symmetric under some transformation, the system is said to be spontaneously broken when one "picks" a vacuum state for this system that is not invariant under the same symmetry transformations as the original Lagrangian. This can be illustrated by the following example. Consider a Lagrangian of the form:

$$\mathcal{L} = T - V = \frac{1}{2}\partial_\mu\phi\partial^\mu\phi - \left(\frac{1}{2}\mu^2\phi^2 + \frac{1}{4}\lambda\phi^4\right) \tag{6}$$

with ϕ being a real scalar field. The first term is the kinetic term (whose interpretation is irrelevant for the discussion of SSB). Just by observation, one can conclude that this Lagrangian is symmetric under a $\phi \to -\phi$ transformation. Now, one can try to find the minimum of this potential V by taking:

$$\frac{\partial V}{\partial \phi} = 0 \implies \phi\left(\mu^2 + \lambda\phi^2\right) = 0. \tag{7}$$

If one requires that $\mu^2 < 0$, this field is minimized by

$$\phi_0 = \pm\sqrt{\frac{-\mu^2}{\lambda}} \equiv v \tag{8}$$

which is called v, the vacuum expectation value of ϕ. A usual procedure is treating perturbative expansions around the ground state, or vacuum state, to establish the dynamics of the system. Expanding ϕ around v according to $\phi = v + \eta(x)$ and inserting it into the expression for the original Lagrangian:

$$\mathcal{L} = \frac{1}{2}\partial_\mu\phi\partial^\mu\phi - \left(\lambda v^2\eta^2 + \lambda v\eta^3 + \frac{1}{4}\lambda\eta^4\right). \tag{9}$$

Without going too much into detail (a thorough derivation is given in both [1] and [2]) one can interpret the term in front of η^2 as a mass term. Thus this Lagrangian describes a particle with mass $m_\eta^2 = 2\lambda v^2 = -2\mu^2$ and the other terms describe the interaction of this particle with other particles and itself. Once the ground state v is chosen, and the expansion around this state is made, it is obvious that this new system is not invariant under the reflection $\phi \to -\phi$, and thus the symmetry of the system is said to have been spontaneously broken. In the following subsection, the same procedure as above will be performed, but for other fields, and similarly mass terms will appear.

SSB and the Higgs Mechanism

Instead of considering the simple real scalar field as was done above, one can consider a complex scalar $SU(2)_L$ doublet which we will call our Higgs field:

$$\phi = \begin{pmatrix} \phi^+ \\ \phi^0 \end{pmatrix}, \quad \phi^+ = \frac{\phi_1 + i\phi_2}{\sqrt{2}}, \quad \phi^0 = \frac{\phi_3 + i\phi_4}{\sqrt{2}}. \tag{10}$$

The Lagrangian has the form:

$$\mathcal{L} = (\partial_\mu \phi)^\dagger (\partial^\mu \phi) - \mu^2 \phi^\dagger \phi - \lambda(\phi^\dagger \phi)^2 \tag{11}$$

which is invariant under the local gauge transformation: $\phi(x) \to \phi'(x) = e^{i\chi(x)}\phi(x)$. The potential in this Lagrangian is the so called Mexican Hat Potential. The ground state of the scalar field is found by minimizing the potential with respect to the fields ϕ^+ and ϕ^0 as before:

$$\phi^\dagger \phi = \frac{-\mu^2}{2\lambda} = \frac{v^2}{2} \tag{12}$$

Now the minimum is chosen, and in this case the standard choice is $\phi_3 = v$, $\phi_1 = \phi_2 = \phi_3 = 0$ so that the field becomes:

$$\phi(x) = \frac{1}{\sqrt{2}} \begin{pmatrix} 0 \\ v \end{pmatrix} \tag{13}$$

The dynamics of the system is determined by expanding around the ground state, and instead of expanding in terms of η as before, we call this new field $H(x)$ which, when quantized, can be interpreted as the *Higgs boson*. In the case of the real scalar field, picking the direction to obtain the ground state resulted in a spontaneously broken symmetry with a massive scalar particle η arising. Similarly, mass terms for scalar particles will arise when plugging in this expression for the field into the original expression for the Lagrangian in Equation (11), where the ∂_μ is replaced with the covariant derivative in Eq. 5. After the dust has settled, one can collect the quadratic terms in the gauge fields:

$$(\mathcal{D}_\mu \phi)^\dagger (\mathcal{D}^\mu \phi) = m_W^2 W^{+\mu} W_\mu^- + \frac{1}{2} m_Z^2 Z^\mu Z_\mu \tag{14}$$

where $W_\mu^\pm = \frac{1}{\sqrt{2}}(W_\mu^1 \mp i W_\mu^2)$ and $Z_\mu = (g_1 W_\mu^3 - g_2 B_\mu)/\sqrt{g_1^2 + g_2^2}$ and lo and behold, the electroweak gauge bosons acquired masses! This was a short and too technical foundation to the popular scientific expression that states that particles acquire mass by interacting with the Higgs boson.

2 Beyond the Standard Model

Theoretical extensions of the Standard Model are proposed to account for some of the unexplained phenomena this universe exhibits. Motivations for Beyond Standard Model (BSM) formulations include questions such as why can the fourth force, gravity, not be accounted for in the SM, why is there more matter than

anti-matter in the universe, what is dark matter and dark energy? One open question that is of particular interest in this analysis is the one concerning neutrinos. The Standard Model along with early experiments have previously proposed that neutrinos are massless, but recent neutrino oscillation experiments [3] provide proof for tiny, but non-zero, neutrino masses. Several extensions of the SM are formulated to address the problem of neutrino masses, and why they are so tiny in comparison to other fermions. Some of them include the proposed existence of a doubly-charged scalar which plays the leading role in this analysis.

Left-Right Symmetric Models

In Sec. 1.1, the introduction of the SM Lagrangian, leptons were put into left-handed $SU(2)$ doublets and right-handed singlets. In the brief explanation, the peculiar property of the SM that does not incorporate right-handed neutrinos, was overlooked. The Left-Right Symmetric Models (LRSM) [4] generate a neutrino mass term by extending the gauge group to include a right-handed $SU(2)_R$ group:

$$SU(2)_L \times SU(2)_R \times U(1)_{B-L} \tag{15}$$

The motivation for this model is the so called See-Saw mechanism that generates light left-handed neutrino masses but heavy right-handed neutrino masses. In the same way that the Higgs mechanism breaks the electroweak symmetry that results in generating the electroweak gauge bosons, the breaking of the LRSM gauge group generates scalar triplets of $SU(2)_R$. What is of interest for this analysis is the doubly-charged scalars that are contained in these $SU(2)_R$ triplets.

Higgs Triplet Model

The Higgs Triplet Model (HTM) is a minimal extension of the SM that adds a complex scalar $SU(2)_L$ triplet. The model provides masses for neutrinos without introducing right-handed neutrinos. The model has 7 Higgs bosons, neutral, singly and doubly-charged.

Doubly-charged Scalars

The doubly-charged scalars that are proposed in some SM extensions can be produced through a virtual photon or a Z-boson as depicted in Fig. 1. Depending on the model, these doubly-charged scalars can either decay directly into same-sign (SS) lepton pairs or into singly charged scalars and virtual W bosons. The decay into a same-sign lepton pairs leads to a very clean signal and is treated in this analysis. The decay rate for doubly-charged scalars to a pair of same-sign leptons is given by [5]:

$$\Gamma(H^{\pm\pm} \to l_i^{\pm} l_j^{\pm}) = S\frac{m_{H^{\pm\pm}}}{8\pi}|h_{ij}|^2 \tag{16}$$

where i and j denote the lepton flavour, $S = 1(2)$ for $i = j$ $(i \neq j)$ and h_{ij} is the Yukawa couplings.

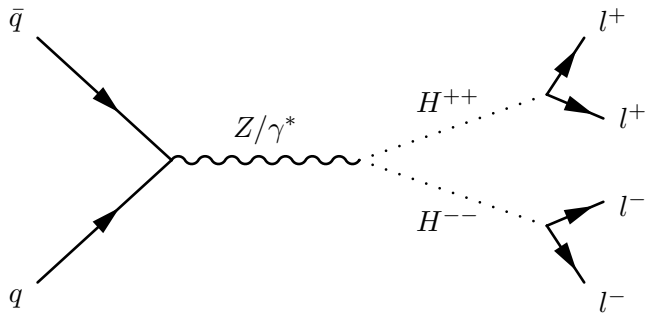

Figure 1: A diagram depicting a process with two doubly-charged Higgs bosons decaying to two same-sign leptons pairs.

3 Experimental Particle Physics at the LHC

The previous sections lead the reader through the theoretical foundations of particle physics, the SM and the BSM extensions introduced to account for the unexplained phenomena in the universe. But, the formulation of the SM could not have been done without close connections to experimental results, and the theories would have been worthless without their testability. The basic idea is to produce all of these fundamental particles by colliding two beams of hadrons (such as protons) or electrons and positrons and observe what comes out. In this section, I will present the structure of particle production through collisions, the Large Hadron Collider (LHC) at CERN, and the ATLAS detector.

3.1 Particle Production at Hadron Colliders

Protons are hadrons, i.e. composite, color neutral particles that are made out of quarks and bound together by gluons. The quarks and gluons (collectively called partons) each carry some fraction of the protons momentum x_{parton}, according to the Parton Distribution Function (PDF), denoted $f(x)$. The momentum of the proton is denoted P and thus a parton carries momentum according to $p = xP$. The likelihood for producing a kind of particle or a particular final state is denoted as the cross section. The hadronic cross section $\sigma_{hadronic} = \sigma_{pp' \to H^{++}H^{--}}$ for pair producing doubly-charged Higgs bosons at the LHC by colliding protons with momentum P and P' is found by considering the partonic cross section for the sub-process $\sigma_{partonic} = \sigma_{q\bar{q} \to \gamma^*/Z^* \to H^{++}H^{--}}$ and the PDF's for finding a quark and an anti-quark in the proton with a certain fraction of the protons momentum, integrated over all of the possibilities for the fractions x_{parton}:

$$\sigma_{q\bar{q} \to H^{++}H^{--}}(P, P') = \sum_q \int_{x_{q,min}}^1 dx_q \int_{x_{\bar{q},min}}^1 dx_{\bar{q}} f_q(x_q) f_{\bar{q}}(x_{\bar{q}}) \sigma_{q\bar{q} \to H^{++}H^{--}}(x_q P, x_{\bar{q}} P') \tag{17}$$

The partonic cross section can be calculated by considering the Lagrangian describing this interaction, or more particularly, by considering the probability amplitude for a transition from an initial state to a desired

final state given by the interaction terms in the Lagrangian. One has to also take into account momentum conservation and masses of the particles involved in the process, all of this is described in [2].

3.2 The Large Hadron Collider

The most famous and powerful hadron collider today is the LHC at the European Organization for Nuclear Research, CERN, located outside of Geneva on the Franco-Swiss border. The LHC is designed to accelerate and collide protons at a center of mass energy of $\sqrt{s} = 14\,\text{TeV}$. Up until now, the LHC has been operated up to $\sqrt{s} = 8\,\text{TeV}$ during Run I until the end of 2012, and after an upgrade, the LHC will operate at its' design energy during Run II starting in 2015. The protons are obtained by stripping off the electrons from hydrogen atoms. The acceleration of the protons is done by a series of accelerators, the linear accelerator Linac 2 followed by the three synchrotrons: the Proton Synchrotron Booster, the Proton Synchrotron (PS) and the Super Proton Synchrotron (SPS). Once the protons have reached an energy of 450 GeV they are injected into the LHC ring in two counter-rotating beams. The LHC ring measures 27 km in circumference and is built up by alternating curved segments with straight segments. There are 8 curved segments in which the protons are bent in a circular orbit by strong magnetic fields, and there are 8 straight segments in some of which the protons are accelerated using time-varying radio frequency electric fields, so called RF cavities. During the acceleration, the protons will enter the RF cavities with different energies. The principle behind using a time-varying electric field is that the relatively slower protons, with lower energy since they bent more in curved segments, arrive earlier relative the other protons in the RF cavity and will thus experience a higher field strength. This gives the slower protons a push forward while the more energetic protons are less accelerated. After some time the proton bunches are separated in time by for example 25 ns (which is the designed bunch spacing for Run II). Once these bunches have reached their intended energy, the two counter rotating beams are focused to collide. The collisions happen at different Interaction Points (IPs) along the LHC ring and each IP is surrounded by a detector to analyze the result of the collisions. There are four main detectors, ATLAS (A Toroidal LHC Apparatus), ALICE (A Large Ion Collider Experiment), CMS (Compact Muon Solenoid) and LHCb.

Luminosity

In order to know how many protons that actually are collided, the concept of luminosity is introduced. It is a measure of how many protons are passing each other per unit time per unit area[15]. The concept of luminosity is also related to the cross section, and therefore the theory through:

$$N = \sigma \int_0^\tau L dt \tag{18}$$

As an experimental physicist, one is interested in the quantity N, the number of events produced, given a certain cross section σ at a given luminosity L of the machine that has been running for some time τ. Therefore the equation shows the important relationship between experimentally produced events, theoretically calculated cross sections and accelerator design. Integrated luminosity is a commonly used

quantity related to the amount of data collected and has the units of cm^{-2} or more conveniently in barns[3] such as fb^{-1}. For example, all of the $\sqrt{s} = 8\,\mathrm{TeV}$ data collected by the ATLAS detector during 2012 is $20.3\,\mathrm{fb}^{-1}$.

3.3 The ATLAS Experiment

The ATLAS detector is designed as a multi-purpose detector aimed to search for many different types of new physics, such as Supersymmetry, dark matter etc. In each successful collision of protons, called an *event*, there is an infinity of possible outcomes. The typical elements that are produced in an event are *jets* of hadrons, which is the result of the hadronization of the available partons after a collision, as well as electrons, muons and tauons and their corresponding neutrinos. A detector must be designed to detect and identify each of the possible resulting particles, as well as measuring their kinematics. The ATLAS detector is built up by several layers of detectors wrapped around some of the beam centred around the interaction point, see Fig. 2.

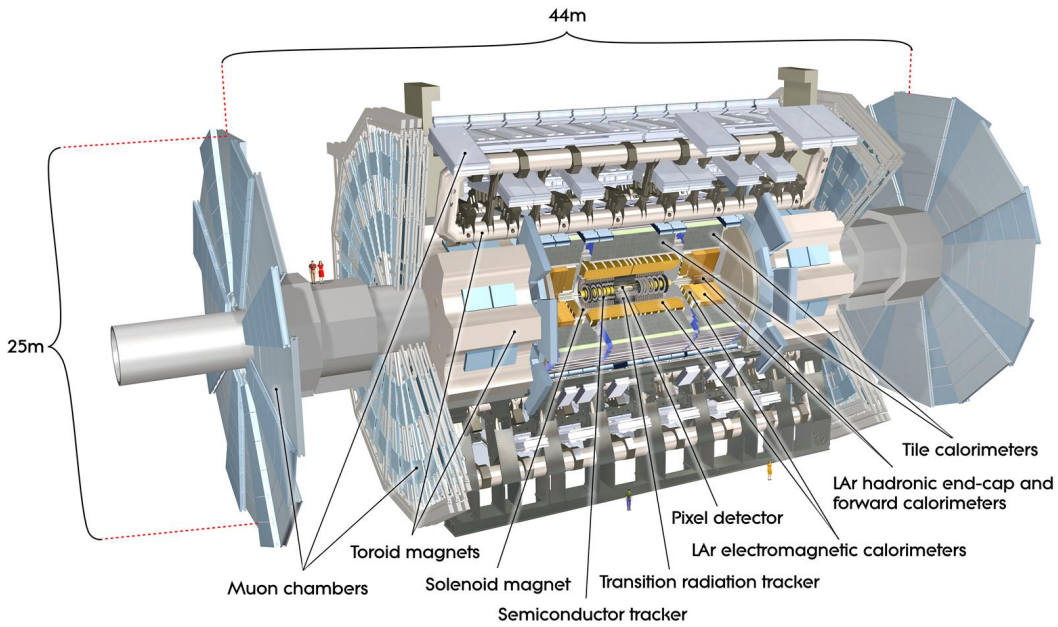

Figure 2: A schematic picture showing the different components of the ATLAS detector [6]

The Inner Detector

The innermost layer is the Inner Detector (ID) designed for measuring the momenta of charged particles as well as their trajectories [7]. Closest to the beam pipe is the Pixel Detector, a silicon based detector,

[3] A barn is a unit of area, $1\,\mathrm{b} = 10^{-24}\mathrm{cm}^2$

designed to determine the impact parameter and identify short-lived particles that decay close to the primary vertex (the vertex in which all the interesting physics happens). The Semiconductor Tracker is also a silicon based detector that measures the momentum of charged particles, the impact parameter and determines the position of the primary vertex. The Transition Radiation Tracker (TRT) uses drift tubes, or *straws*, filled with a gaseous mixture of xenon, carbon dioxide and oxygen. Charged particles ionize the gas in the tubes and the freed electrons drift to an anode which can be used to determine the track coordinate and momentum of the charged particles. The TRT has the ability to identify particles by discriminating between different charged particles such as the pion and the electron. The whole ID is subject to a magnetic field of 2 T generated by a solenoid.

The Calorimeters

Outside of the ID are different calorimeters whose main purpose is to measure the energy of the particles [8]. The idea is that the particles should deposit all of its energy into the calorimeter, which means that the detector should be filled with materials in which the particles are likely to interact. The first type of calorimeter is the Electromagnetic Calorimeter, which is a lead-liquid argon detector for measuring the energy of and identifying electrons, positrons and photons. The second type of calorimeter is the hadronic calorimeter which is composed out of three different kinds of calorimeters, the tile calorimeter, the hadronic end-cap calorimeter and forward calorimeter (which has both an electromagnetic part and a hadronic part). The hadronic calorimeter enables determination of the energy of hadrons.

The Muon Spectrometer

Due to their relatively long life time, muons are able to pass through the inner detectors and calorimeters, and are identified in the outermost detector, the muon spectrometer [9]. A magnetic field generated by a toroid enables for momentum measurement and charge identification. This is due to the fact that these charged particles will bend in a magnetic field, and since the radius of curvature is related to their momentum. Drift tubes are used for tracking. The muon spectrometer measures the momentum of muons, which is of essence in this analysis. The momentum resolution is examined in [10] by considering the invariant mass spectrum of the Z boson, the Z-peak, and shows that the resolution $\sigma(p_{\mathrm{T}})/p_{\mathrm{T}}$ becomes worse with higher p_{T}. The momentum resolution can further be translated into invariant mass resolutions, which is relevant in this analysis, since the aim is to find a mass peak, i.e. an invariant mass distribution. Muons are identified by using information from the ID and the muon spectrometer.

4 Search for doubly-charged Higgs boson

Now the essence of this thesis is swiftly approaching. After the theoretical motivation behind BSM searches and the presentation of the ATLAS detector, the aim of this thesis can be formulated. Searches for doubly-charged Higgs bosons in same-sign dilepton final states have been conducted at CMS [11] and ATLAS [12] at $\sqrt{s} = 7\,\mathrm{TeV}$, at the LHC. Lower bounds on the mass of the doubly-charged Higgs bosons have been established between 204 and 459 GeV [11] and between 375 and 409 GeV [12] assuming a 100 % branching

ratio for each final state, ($e^{\pm}e^{\pm}$, $e^{\pm}\mu^{\pm}$, $\tau^{\pm}e^{\pm}$, $\mu^{\pm}\mu^{\pm}$, $\mu^{\pm}\tau^{\pm}$, $\tau^{\pm}\tau^{\pm}$ for [11] and $e^{\pm}e^{\pm}$, $e^{\pm}\mu^{\pm}$, $\mu^{\pm}\mu^{\pm}$ for [12]). In a dissertation published in 2014, [13] , with an inclusive search for the production of same-sign lepton pairs ($e^{\pm}e^{\pm}$, $e^{\pm}\mu^{\pm}$, $\mu^{\pm}\mu^{\pm}$) using 20.3 fb^{-1} of $\sqrt{s} = 8$ TeV pp collision data recorded with the ATLAS detector, lower mass limits on doubly-charged Higgs bosons were further improved from the $\sqrt{s} = 7$ TeV by 30-40 % (470-550 GeV for left handed[4] Higgs bosons and 370-440 GeV for right handed Higgs bosons). With the starting point in this analysis [13], the aim of my thesis is to improve the lower mass limits by implementing new optimized cuts to reduce the background while keeping the signal.

4.1 Event Generators

In order to do particle physics analyses, it is essential to compare the recorded data to theoretical expectations. The connections between experimentally recorded data and theory are event generators. The idea behind event generators is to simulate what an event would look like. In essence, the event generators provide complete information about what the event would look like, if it occurred. The simulations are done by using the Monte-Carlo method, which is based on generating random samples to obtain numerical results, and more specifically in the particle physics case, evaluate integrals over probability density functions and generate samples according to these distributions. In the case of the optimization done in this thesis, the idea is to use doubly-charged Higgs boson simulations and simulations of ordinary SM background processes, and find variables to cut on so that the background is minimized. When these cuts are established, they are applied to real data. If a significant excess of data is observed in the region where the background is minimized, this might indicate a discovery.

4.2 Optimization

As mentioned in the previous subsection, the idea behind the optimization is to find variables to cut on to reduce the SM background while keeping a significant part of the signal. Significance is measured in standard deviations n_σ, assuming a Normal (or Gaussian) distribution $N(\mu, \sigma)$ which is the probability that the measured value x will cover the true value μ [16]. For example, a "1σ" ($n_{sigma} = 1$) effect corresponds to an area of 0.32 of the upper tail outside of $\delta = 1\sigma$ from the mean μ, which means that once every third time a measurement is conducted the true value will fall outside the confidence interval. A "3σ" ($n_{sigma} = 3$) effect corresponds to an area of the upper tail outside of $\delta = 3\sigma$ of 0.0027, which means that once every 370th time a measurement is conducted the true value will fall outside the confidence interval. An effect is considered significant when $n_\sigma > 5$. The significance in this analysis is defined as:

$$n_\sigma = \frac{N_S}{\sqrt{N_B}} \tag{19}$$

[4]Left and right-handed refers to the chirality of the particle, see Section1.1. In this case, the left-handed and right-handed doubly-charged Higgs bosons decay into a pair of left-handed or right-handed fermions respectively.

where B is the simulated number of background events, and S the simulated number of signal events. This quantity is also related to the Luminosity L introduced in Eq. 18:

$$N = \sigma \int_0^\tau L dt \tag{20}$$

where one can relate the cross sections of the signal and background processes, σ_S and σ_B, and thus calculate the amount of data needed to reach $n_{sigma} > 5$ which would mean detection of the signal, in terms of integrated luminosity L_{int}:

$$n_\sigma = \sqrt{L_{int}} \frac{\sigma_S}{\sqrt{\sigma_B}}. \tag{21}$$

4.3 same-sign Event Selection

This analysis is done by assuming that the doubly-charged Higgs boson only decays to muons, thus ignoring bosonic decays such as $H^{\pm\pm} \to W^\pm W^\pm$ and other leptonic final states[5]. The assumption provides a clear di-lepton final state free of SM background, ideal for analyses, as opposed to the bosonic decays with complicated final states including missing transverse momentum due to neutrinos[6] and jets. Under this assumption, one can conclude that the signal final state event should include pairs of same-sign muons with high transverse momentum ($p_{\mathrm{T}} > 20\,\mathrm{GeV}$), originating from or close to the primary vertex (prompt muons) as well as being isolated (meaning that a small cone surrounding the track is free from other tracks from jets other processes). All the cuts are presented in Appendix A.3. The Monte-Carlo samples used for the five signal regions are presented in Appendix A.4.

4.4 same-sign Background

The perks of the assumed 100 % branching ratio to same-sign leptons is that it provides a clean signal with low background predictions. The dominant SM background processes that imitate the signal, i.e. with a final state with two same-sign leptons, are the following:

- $W^+Z \to l^+ \nu\, l^\pm l^\mp$ (a)
- $W^-Z \to l^- \bar{\nu}\, l^\pm l^\mp$ (b)
- $ZZ \to l^- l^- l^+ l^+$ (c)

These processes are presented as diagrams in Fig. 4.

There are also processes where a $t\bar{t}$-pair is produced and decays semi-leptonically along with a gauge boson (either W^+ or Z) that decays leptonically, see Fig. 5. Another possible SM background is $W^\pm W^\pm \to l^\pm l^\pm \nu\nu + 2\mathrm{jets}$. The cross sections for these processes are presented in Appendix A.4.

[5] Leptonic final states such as $H^{\pm\pm} \to e^\pm e^\pm / \tau^\pm \tau^\pm$ and lepton flavour violating processes such as $H^{\pm\pm} \to e^\pm \mu^\pm / e^\pm \tau^\pm / \mu^\pm \tau^\pm$.

[6] Neutrinos cannot be detected directly in the ATLAS detector, but by imposing conservation of momentum their existence can be indirectly detected by assigning them the "missing" momentum.

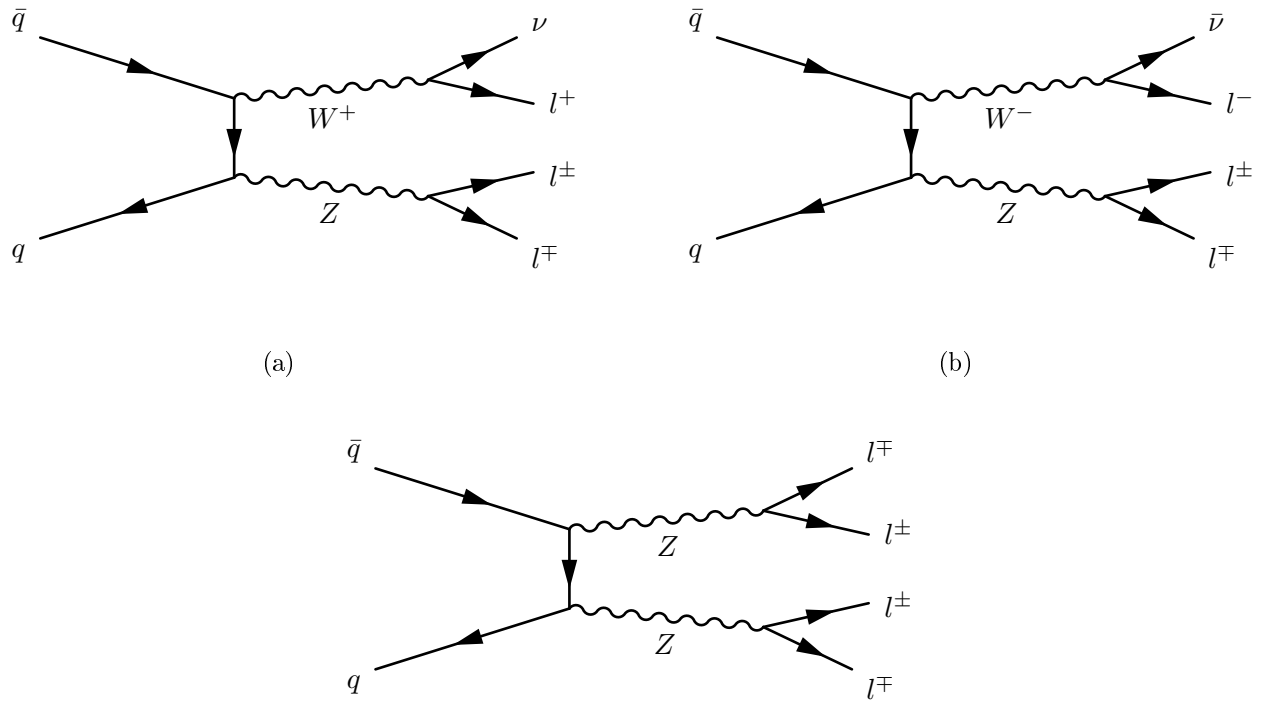

(a) (b)

(c)

Figure 4: Examples of some of the dominant SM background processes producing same-sign leptons, $W^+Z \to l^+\,\nu\,l^\pm\,l^\mp$ (a), $W^-Z \to l^-\,\bar{\nu}\,l^\pm\,l^\mp$ (b) and $ZZ \to l^-\,l^-\,l^+\,l^+$ (c).

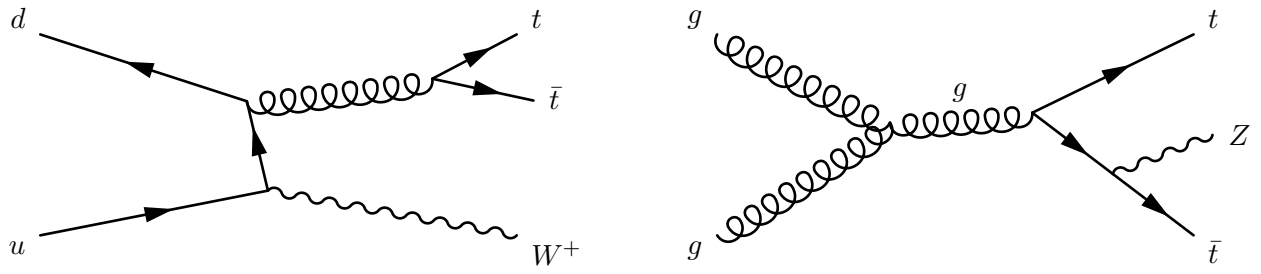

(a) (b)

Figure 5: Examples of some of the more rare SM background processes producing same-sign leptons, $t\bar{t} + W^+$ (a) and $t\bar{t} + Z$ (b), the t and $\bar{t}$ can decay to muons, and the W^+ and Z can also decay to muons, and combined they produce at least one same-sign lepton pair.

Fake Factor Method

The processes mentioned in the previous subsection are so called prompt processes, i.e. the leptons in the final state come from the primary interaction. There is another kind of process that can lead to same-sign lepton pairs in the final state. These processes are called non-prompt, they provide same-sign muon pairs in the final state where either one or both of the muons does not originate from the primary interaction (called *true* fakes), or from either photons, jets or hadrons being misidentified as muons (just called fakes) (this misidentification is a much smaller effect than the non-prompt secondary muons). The dominant non-prompt process, the true fakes, are decay products from b-jets, pions or kaons produced in the primary interaction and decays in flight. For example if some particle with short life time decays to a muon within the distance set by the impact parameter d_0, it can wrongly be identified as a signal muon even though it is not originating from the primary vertex [7]. To estimate the non-prompt contribution to the background, I will use the results of a so called fake factor method [13]. The idea is to predict how many of these muons are non-prompt by, first of all, defining a region that is assumed to be rich in fakes, called the fake region. Since this method is data-driven, one must also impose a fake region that is different than the signal region defined in Appendix A.3. The fake region is defined by loosening the impact parameter cut $|d_0|$, to get a region that is rich in fakes, and by reversing the $|d_0|/\sigma(d_0)$ to get a region that is different than the signal region. The fake region is defined by:

- $|d_0|/\sigma(d_0) > 3$
- $|d_0| < 10\,\text{mm}$

Now, one defines two objects, numerator and denominator objects. Numerator objects are defined as signal muons but in the fake region. Denominator objects are defined as numerator objects, but with one cut reversed to make numerator and denominator objects mutually exclusive. The ratio $f \equiv \frac{n_N}{n_D}$ is the "fake factor" calculated by measuring the number of numerator objects n_N and denominator objects n_D, both measured in p_T and η binning. The fake factor can be viewed as a ratio that gives how many denominator objects will appear as signal muons in some region defined by p_T and η. The fake factors are calculated in [13] and presented in A.5. To estimate the background contribution due to fakes, this fake factor is applied to different scenarios where one or both of the "muons" in a muon pair pass/passes the denominator cut, and thus scaled one finds out how many of these denominator objects are actually signal muons. Theoretically, there are three types of scenarios, namely

- Type A: Only the leading[8] muon is fake.
- Type B: Only the sub-leading muon is fake.
- Type C: Both the leading and sub-leading muons are fakes.

When evaluating this experimentally, one encounters scenarios where all muons in an event are paired up in all possible combination, and within these pairs, either both pass the numerator cuts (N+N), the leading

[7] See Appendix A.3

[8] The leading muon is the muon with highest p_T.

one passes the numerator cut and the sub-leading passes the denominator cut (N+D), the leading one passes the denominator cut and the sub-leading passes the numerator cut (D+N) or both the leading and sub-leading pass the denominator cut. The total number of fakes is obtained by adding the contributions from the three theoretical scenarios, A+B+C, which experimentally is translated to the following:

$$n_{Fakes} = \sum_{i\in(N+D)} f_2(p_{Ti},\eta_i) + \sum_{i\in(D+N)} f_1(p_{Ti},\eta_i) - \sum_{i\in(D+D)} f_1(p_{Ti},\eta_i) f_2(p_{Ti},\eta_i)$$

where the first term contains contributions from types B and C (the sum $\sum_{i\in(N+D)}$ is over muon pairs where the leading muon passes the numerator cuts and the sub-leading passes denominator cuts with f_2 being the fake factor for the sub-leading muon, that provides how many of these muons can be interpreted as fake muons), the second term contains contributions from type A and C (the sum $\sum_{i\in(D+N)}$ is over muon pairs where the leading muon passes the denominator cuts and the sub-leading passes numerator cuts with f_1 being the fake factor for the leading muon, that indicates how many of these muons can be interpreted as fake muons), and the last term is included to avoid double counting of the contributions from type C. In [13], the η dependence on the fake factors is not significant, and therefore the p_{T} dependence of the fake factor will be considered.

4.5 Strategy

Now that the aim of this thesis is formulated, along with the description of the signal and background processes, the strategy for this analysis is presented. As mentioned above, the idea is to improve the lower mass limits by finding optimized cuts that reduce the background while keeping the signal, and then apply these cuts to real data. The data used are collected at the LHC during Run I at $\sqrt{s} = 8\,\mathrm{TeV}$, and correspond to an integrated luminosity of $20.3\,\mathrm{fb}^{-1}$. The variables to cut on that are examined are: the transverse momentum p_{T} of the leading and sub-leading muons, the scalar sum H_T of the lepton transverse momenta, the angular difference $\Delta\phi$[9] , pseudo-rapidity η, missing transverse momentum $\not{E}$ and invariant mass of the muon pair. In principle, a cut on the number of same-sign lepton pairs could be examined (since theoretically more than one same-sign pair could be produced), but according to recent publications [14], multi-lepton final states are heavily suppressed. Events with two or more same-sign muons are selected, and all pair combinations of muons are considered. The analysis is performed as a so called *blind* analysis, which means that in principle the whole analysis is made with just considering MC samples, i.e. without looking at data. This is to reduce the probability for biasing the optimization due to what is seen in data. Once the cuts are obtained, the analysis is "unblinded" when the cuts are applied to data. Only statistical errors are considered, systematic errors are for the most parts ignored in this analysis (see Appendix A.2 for a presentation of the uncertainties).

[9] ϕ is the azimuthal angle which is the angle that sweeps out the $x-y$ plane, perpendicular to the beam axis z and $\Delta\phi = \phi_1 - \phi_2$ is the difference in azimuthal ϕ between the two muons.

5 Results

This section is organized as follows. I will first give a couple of remarks on the mass points used, and comment on the event selection. Then the properties of the different background and signal processes are presented, followed by a description of the variables that have been examined and the final optimized cuts and the corresponding significances. The numerical results are presented at the end of this section.

5.1 Remarks

This analysis was performed using five different mass points, i.e. MC samples generated for a doubly-charged Higgs boson of mass $m_{H^{\pm\pm}} = 150\,\text{GeV}$, $m_{H^{\pm\pm}} = 300\,\text{GeV}$, $m_{H^{\pm\pm}} = 500\,\text{GeV}$, $m_{H^{\pm\pm}} = 600\,\text{GeV}$ and $m_{H^{\pm\pm}} = 1000\,\text{GeV}$. Even though a doubly-charged Higgs boson has been excluded up to a certain mass (400-500 GeV, see Sec. 4.), I chose to include the mass points $m_{H^{\pm\pm}} = 150\,\text{GeV}$ and $m_{H^{\pm\pm}} = 300\,\text{GeV}$ because they correspond to processes having larger cross sections and narrower mass resolutions than the higher mass points, and thus provide more statistics to simplify the optimization. In ATLAS analyses there are a couple of corrections that are applied to Monte-Carlo (MC) samples, to account for, e.g., pile-up effects, lepton identification and isolation efficiencies, for better agreement with data. In this analysis, these corrections are not applied, but instead the MC samples are normalized to data. The normalization is done before any cuts are applied. Remarks on the data taken as well as the a comment on the uncertainties included in this analysis are presented in Appendix A.1 and Appendix A.2. The actual analysis was performed using the data analysis framework ROOT [20] developed for high energy physics analyses.

5.2 Signal and Background Distributions

Below are the background and signal distributions presented. The relevant variables for this analysis (as will be discussed below) are the leading muon p_{T}, invariant mass of the muon pair and their $\Delta\phi$ distribution.

Non-Prompt Background

The background contribution from non-prompt[10] muons is presented in Fig. 6, showing the invariant mass distribution for muon pairs in prompt and non-prompt background processes, as well as data. The histograms show a reasonably good agreement between the total background (prompt + non-prompt) and data, which justifies the use of the fake factor method in this region.

[10] From now on I will use the terms *fakes* and *non-prompt* interchangeably.

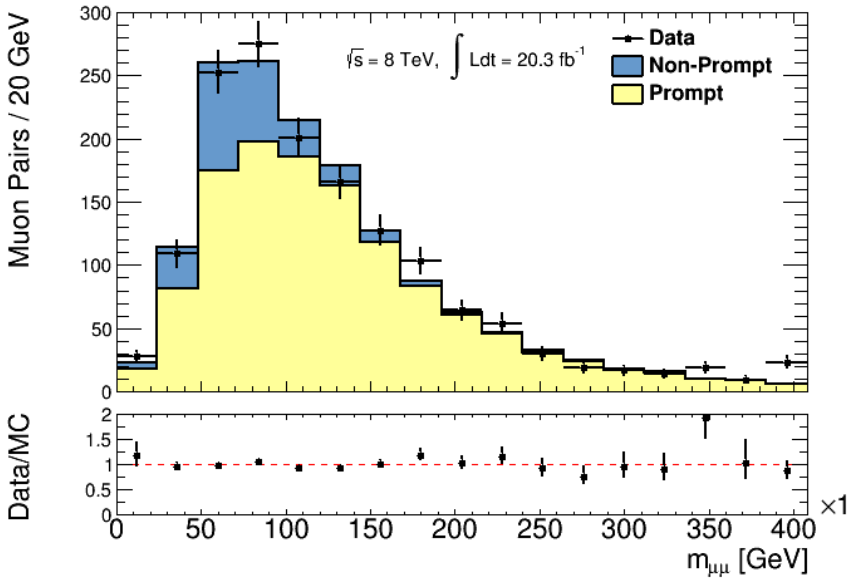

(a)

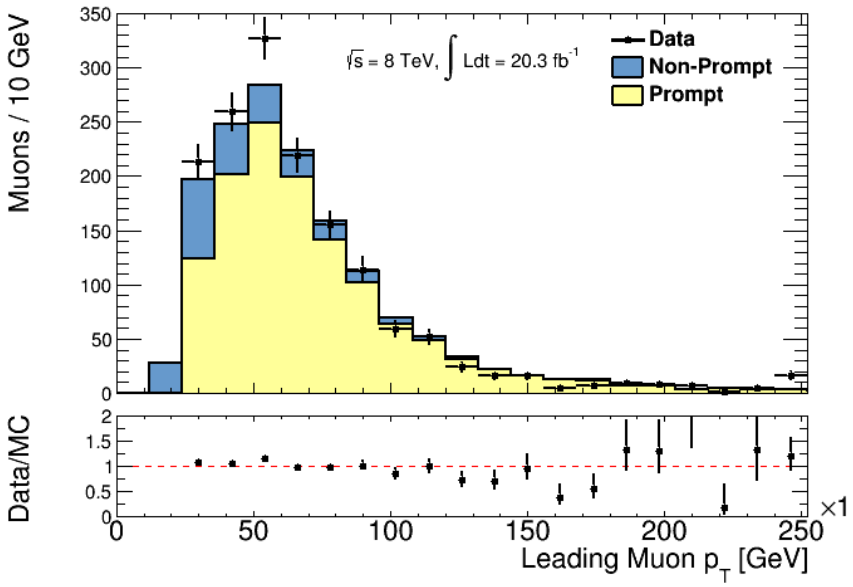

(b)

Figure 6: Invariant mass distribution for muon pairs (a) and leading muon p_{T} distributions (b). The stacked histograms represent the background composed of prompt and non-prompt muons. The data are shown as closed circles with Poisson errors. The last bin is an overflow bin. The ratio plot shows the agreement of MC to data with Poisson errors.

Prompt Background

The prompt SM distributions are presented in Fig. 7 and Fig. 8 for the three relevant variables in this analysis. The most dominant background are the diboson processes ($W^{\pm}Z \rightarrow l^{\pm}\nu l^{\pm}l^{\mp}$, $ZZ \rightarrow l^{-}l^{-}l^{+}l^{+}$). It is worth mentioning is that the SM backgrounds seem to be heavily suppressed at high p_{T}-and mass ranges. The lack of statistics in the MC generated samples in these regions should be taken into account when performing the optimization. Since the aim of the optimization is to reduce the background while keeping the signal, the lack of backgrounds in higher mass regions must be taken into account. At low p_{T} fake muons are dominant.

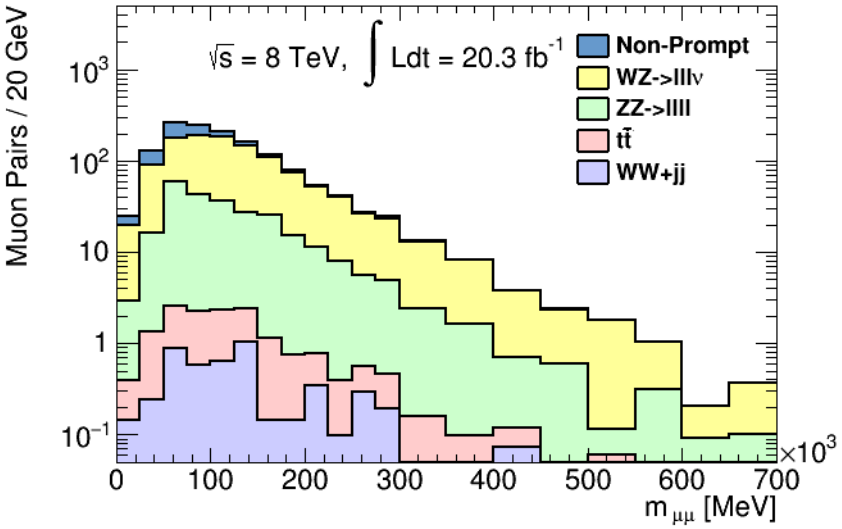

(a)

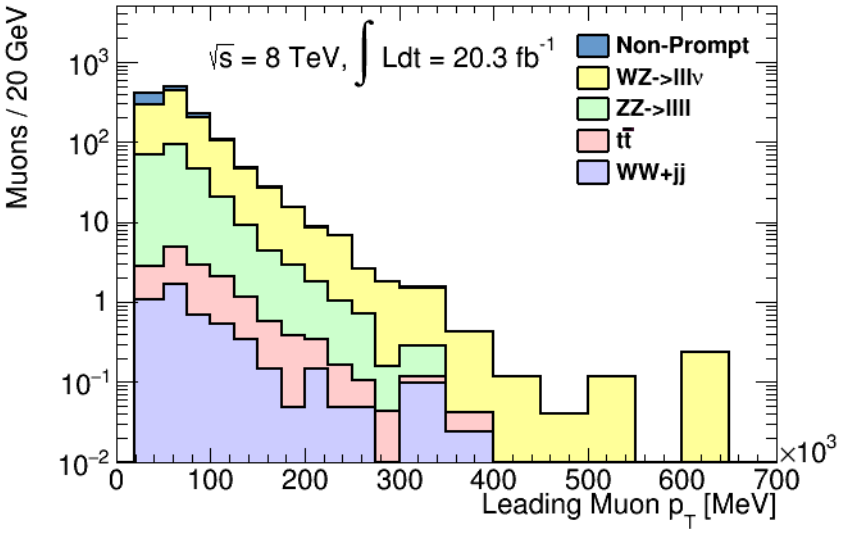

(b)

Figure 7: Invariant mass distribution for muon pairs (a) and leading muon p_{T} distribution for the dominant SM backgrounds represented as stacked histograms. For the invariant mass and p_{T} distributions the binning is changed from 300 GeV to include more statistics.

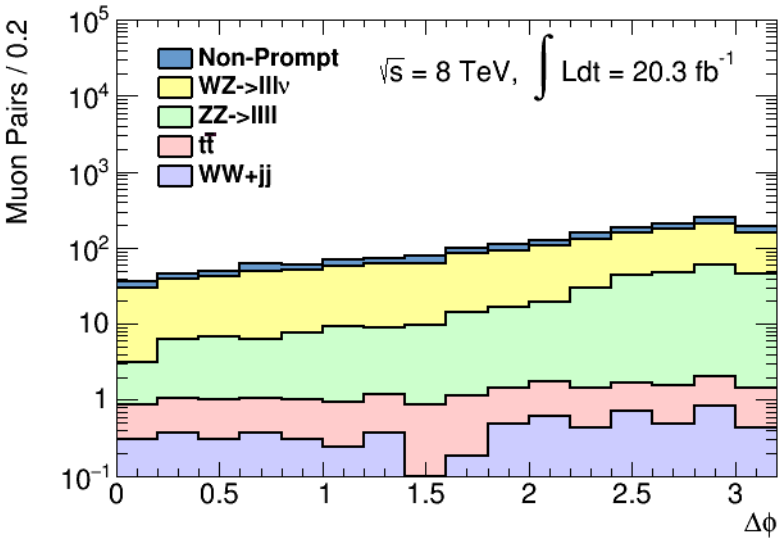

Figure 8: $\Delta\phi$ distribution for the dominant SM backgrounds represented as stacked histograms.

Signal Distributions

The five signal regions are examined in this subsection, the signal regions corresponding to doubly-charged Higgs bosons of masses $m_{H^{\pm\pm}} = 150\,\text{GeV}$, $m_{H^{\pm\pm}} = 300\,\text{GeV}$, $m_{H^{\pm\pm}} = 500\,\text{GeV}$, $m_{H^{\pm\pm}} = 600\,\text{GeV}$ and $m_{H^{\pm\pm}} = 1000\,\text{GeV}$. In Fig. 9 and Fig. 10, the signal distributions are presented with the total background and data. The momentum resolution of the muon spectrometer becomes obvious at this point, with the narrower peaks for lower Higgs masses[11]. Unfortunately, binning with respect to the expected invariant mass or momentum resolutions has not been implemented, only a general broadening of the bins to include more statistic has been implemented at 300 GeV for both distributions.

[11] The broader peaks of the p_{T} and invariant mass distributions for higher Higgs masses could in addition to being a detector effect be due to the shorter lifetimes of the heavier Higgs bosons which will result in broader peaks.

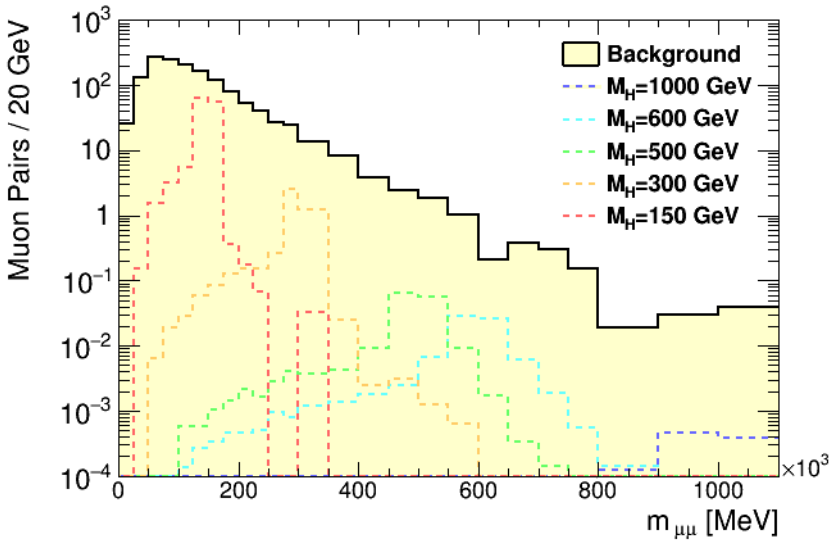

(a)

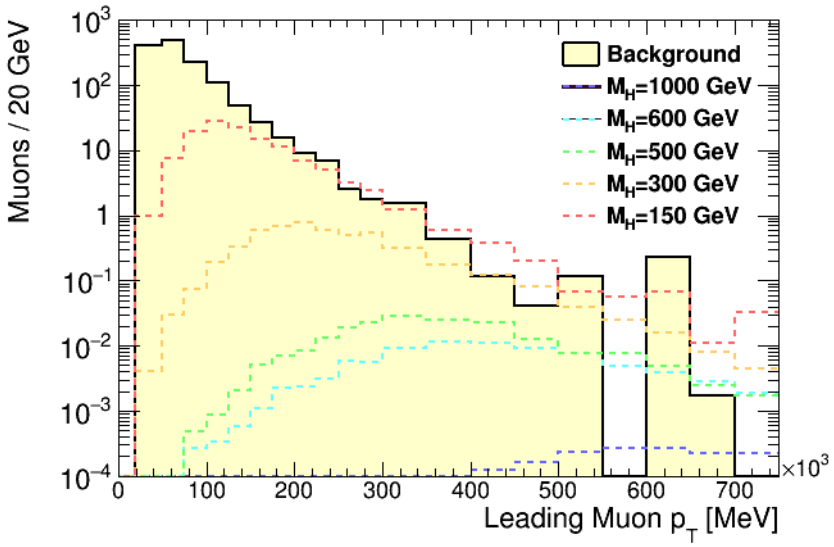

(b)

Figure 9: Invariant mass distribution for muon pairs (a) and leading muon p_{T} distribution (b) for the total background, signal. The signals are represented as hatched lines. The binning is changed from 300 GeV and from 800 GeV, and the last bins are overflow bins.

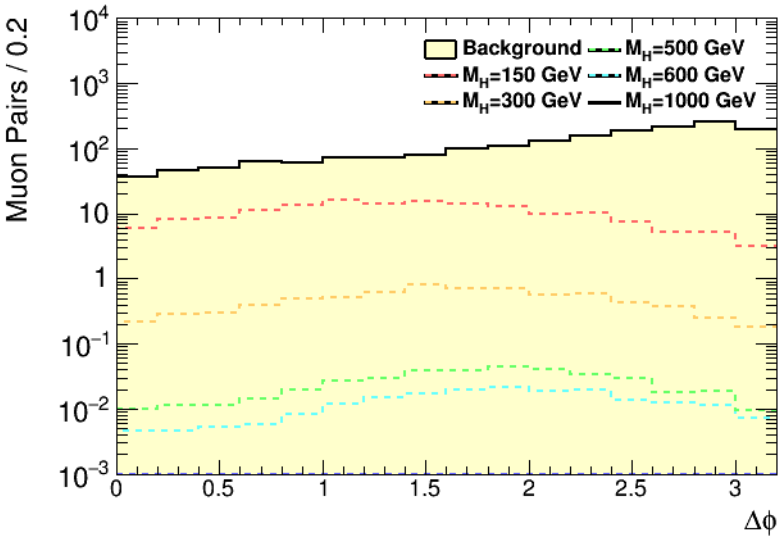

Figure 10: $\Delta\phi$ distribution for the total background, signal and data. The signals are represented as hatched lines.

To find the optimal variables to cut on, and their optimal values, it is essential to find a region in the parameter space where the signal and background differ. From the plots in Fig. 9 and Fig. 10, only the invariant mass and momentum resolution for the signal are obvious. It is also apparent from these plots that the optimization for the higher mass regions is not an easy task, due to the lack of statistics in the background as well as the low cross sections for the signal processes. But zooming in on the scale of the momentum and invariant mass distributions and on the log-scale of the $\Delta\phi$, see Fig. 11, more distinct peaks are unveiled. The choice to include the MC samples for the already excluded doubly-charged Higgs bosons of masses $m_{H^{\pm\pm}} = 150\,\text{GeV}$, $m_{H^{\pm\pm}} = 300\,\text{GeV}$ becomes obvious here. By finding optimal variables to cut on for these signal regions that are characterized by their relatively high cross section, one can extrapolate these results to the higher mass regions as well. From Fig. 11 another cut becomes obvious, a lower cut in p_T around 100 GeV that is predicted to rise for higher mass regions. This cut is heavily correlated to a cut around the expected invariant mass peak of the signal for low p_{T} regions. Examining the difference in azimuthal angles for the two muons, another trend is disclosed. As opposed to the other variables, the $\Delta\phi$ has no lack in statistics in any region, which gives a hint that it should be an interesting variable to include. By eye, one can see that a lot of background can be excluded by setting an upper cut on $\Delta\phi$. The background has high values for the $\Delta\phi$, meaning that the same-sign leptons often go out back-to-back in the detector. Keeping the behaviour of the background in mind, an extrapolation of the $\Delta\phi$ cut can be done by considering the boost of the doubly-charged Higgs bosons. A light doubly-charged Higgs boson will be more boosted than a heavier one. This is because a light Higgs has more available momentum after its production, i.e. it will travel faster and be more boosted. Whereas for the heavier Higgs boson, more of the available energy goes into its production, leaving it with less momentum to travel off with. Therefore

the decay products of the heavier doubly-charged Higgs bosons will go out more back-to-back, i.e. with a higher $\Delta\phi$ value. Extrapolating on this trend of the less boosted heavier Higgs bosons, one can assume that a cut on $\Delta\phi$ that increases with the doubly-charged Higgs mass is in order.

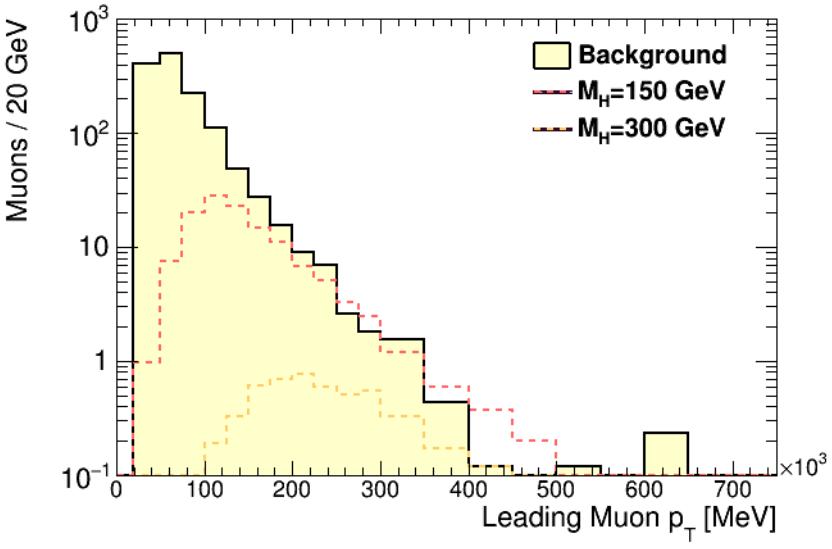

(b)

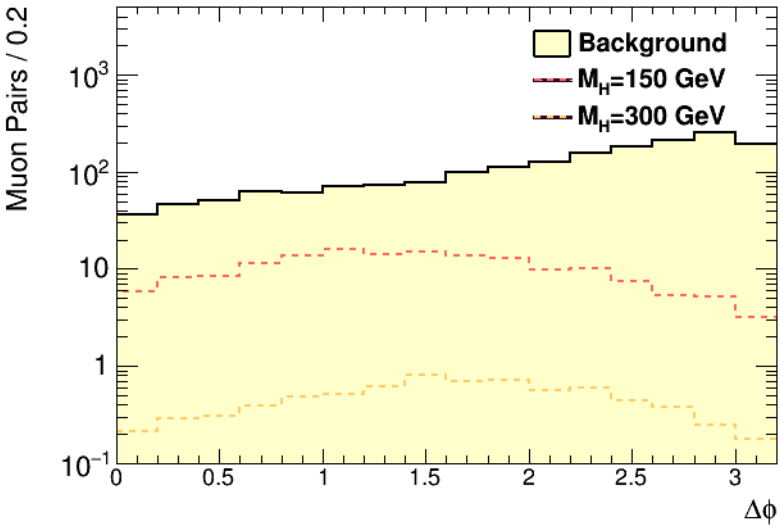

Figure 11: Leading muon p_{T} and $\Delta\phi$ distribution for the total background and signal, zoomed in to disclose the characteristic peaks and bumps of the signal.

5.3 Optimized Cuts

Events are selected with two or more muons. First of all, the most obvious cut is applied, namely the same-sign muon requirement. The events selected are those where two muons have the same-sign, and where more than two muons form combinations of muon pairs that have the same-sign. An invariant mass cut is applied $m_{ll} < 15\,\text{GeV}$ to reject events that could originate from the mass peak of a J/Ψ meson[12][13]. The invariant mass of the decay products of the doubly-charged Higgs boson forms a mass peak centred around the expected mass, see Sec. 5.2. Therefore, an effective way of isolating the signal would be to apply a cut around the mass peak of width Δm_H according to:

$$|m_{ll} - m_H| \leq \Delta m_H \tag{22}$$

where m_{ll} is the invariant mass of the muons and m_H the mass of the doubly-charged Higgs boson. With the starting point in the discussion about resolution of the p_{T} and invariant mass distributions of the muon spectrometer (see Sec. 3.3.), conclusions can be made about the width of the expected mass peaks in the different signal regions. The $\Delta\phi$ cut is applied as well as a cut on leading muon transverse momentum. Several variables were examined in the search for the maximum significance, such as sub-leading muon p_{T}, the pseudo-rapidity[14] η of the leading and sub-leading muon, missing transverse momentum $\not{E}$, number of jets and the scalar sum of lepton p_{T}, H_T[15], but these additional variables were not as effective as the optimal cuts Δm_H, $\Delta\phi$ and p_{T} of the leading muon. The variable η of the leading and sub-leading muon did not provide a good enough discrimination between background and signal. A cut on the number of jets did not improve the results either, since neither the signal nor the background expects a dominant jet contribution. Sub-leading muon p_{T} and H_T showed distributions where no additional discrimination between the signal and background could be made, so they were not used.

For the optimization, a script was written that maximized the significance when making a selection on three of the different variables simultaneously, and provided the optimal values for the three most efficient variables to cut on. Each variable was examined on its own, and rejected if it did not increase the significance. The optimal values for the optimal variables for each signal region are presented in Tab. 1, along with the corresponding significance.

[12] The J/Ψ meson is a bound state of a charm and an anti-charm quark of mass 3.097 GeV with significant branching fraction to leptons that could mimic the signal.

[13] In fact, this cut is a residue from a previous analysis [13] where same-sign electrons are treated in addition to muons. For electrons, the probability for charge misidentification is significantly higher (due to Bremsstrahlung), resulting in a larger probability for the opposite sign decay products of a J/Ψ to be misidentified as a same-sign pair. This effect is heavily reduced for muons since muon charge misidentification is negligible [13], so even though the cut in this analysis is redundant, it is still applied for completeness.

[14] Pseudo-rapidity is defined as $\eta = -\ln(\tan(\theta/2))$ a spatial coordinate describing the angle of a particle relative to the beam axis where θ is the angle from the particle track to the beam axis.

[15] $H_T \equiv \sum_i p_{T,i}$

Cuts	Δm_H (GeV)	p_{T} (GeV)	$\lvert\Delta\phi\rvert$	n_σ (σ)
$\mathbf{m_H = 150\,GeV}$	> 9	> 120	< 1.6	33
$\mathbf{m_H = 300\,GeV}$	> 27	> 130	< 1.2	3.8
$\mathbf{m_H = 500\,GeV}$	> 60	> 130	< 1.5	1.7
$\mathbf{m_H = 600\,GeV}$	> 100	> 130	< 1.7	1.2
$\mathbf{m_H = 1000\,GeV}$	> 250	> 100	< 2.5	0.044

Table 1: Optimized values for the optimal variables to cut on with the associated significance for each signal region. p_{T} is the leading muon transverse momentum.

Bearing in mind the assumptions on the values of the cuts that were discussed above, it is of interest to see if the predicted values correspond to the values obtained by the actual optimization performed by the script. From Tab. 1, the value for Δm_H cut increases with the doubly-charged Higgs mass, which is according to the predicted trend proposed by the invariant mass resolution of the muon spectrometer. The p_{T} cut is not changing drastically, it is maintained around 120 GeV which is opposing the slight rise that was predicted. Another deviation from the predictions is in the relatively low value of the p_{T} cut for m_H of 1000 GeV. This deviation can be explained by the efficiency of the Δm_H cut, which successfully reduces a lot of background resulting in the p_{T} cut becoming more or less useless. The $\Delta\phi$ cut is also following the predicted trends, with a value increasing with the doubly-charged Higgs mass, at least for $m_H = 300$ GeV to $m_H = 1000$ GeV. The high value for the $\Delta\phi$ cut for $m_H = 150$ GeV can probably be explained by the efficiency of the other cuts. Although it is assumed that the $\Delta\phi$ cut is the most sensitive for low doubly-charged Higgs masses, it is still not as efficient as the other cuts in this region. The efficiency in these cuts is cross-checked in the subsequent section treating the numerical results of the efficiency of the cuts. The significances follow the obvious prediction that the significance increases with cross section. The results when only applying the p_{T} and $\Delta\phi$ cuts are presented in Tab. 2 along with the corresponding significance. When only applying the p_{T} and $\Delta\phi$ cuts, the significance is reduced by an order of magnitude, approximately, for all signal regions.

Cuts	p_{T} (GeV)	$\lvert\Delta\phi\rvert$	n_σ (σ)
$\mathbf{m_H = 150\,GeV}$	> 120	< 1.6	12
$\mathbf{m_H = 300\,GeV}$	> 130	< 1.2	0.52
$\mathbf{m_H = 500\,GeV}$	> 130	< 1.5	0.030
$\mathbf{m_H = 600\,GeV}$	> 130	< 1.7	0.016
$\mathbf{m_H = 1000\,GeV}$	> 100	< 2.5	0.00044

Table 2: Optimized values for the $\Delta\phi$ and p_{T} cuts with the associated significance for each signal region.

5.4 Numerical Results

First of all, histograms containing the five signal regions, the total background and the data, with a ratio plot to indicate the agreement between data and background, are presented in Fig. 12 and Fig. 13.

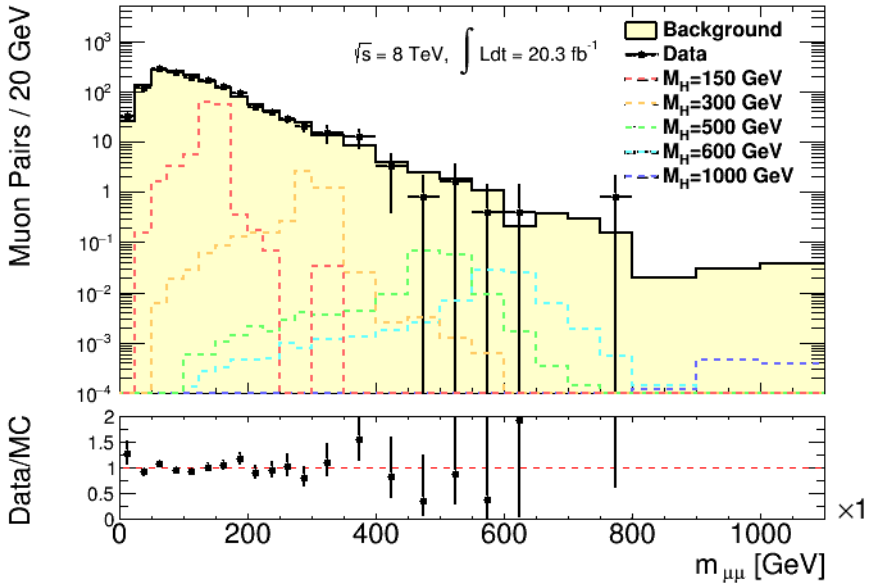

(a)

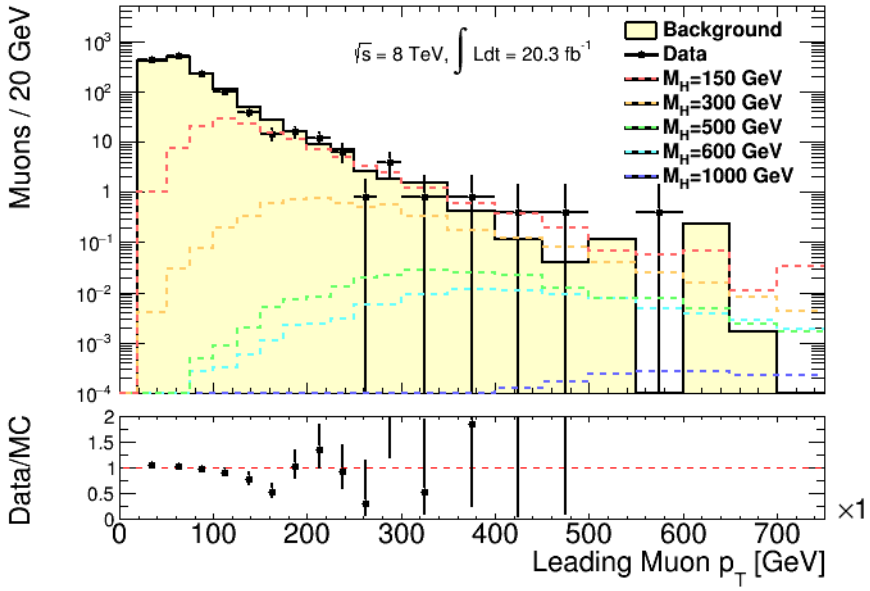

(b)

Figure 12: Invariant mass distribution for muon pairs (a) and leading muon p_{T} distribution (b) for the total background, signal and data. The signals are represented as hatched lines, and the data are represented as closed circles with Poisson errors. The binning is changed from 300 GeV and from 800 GeV, and the last bins are overflow bins.

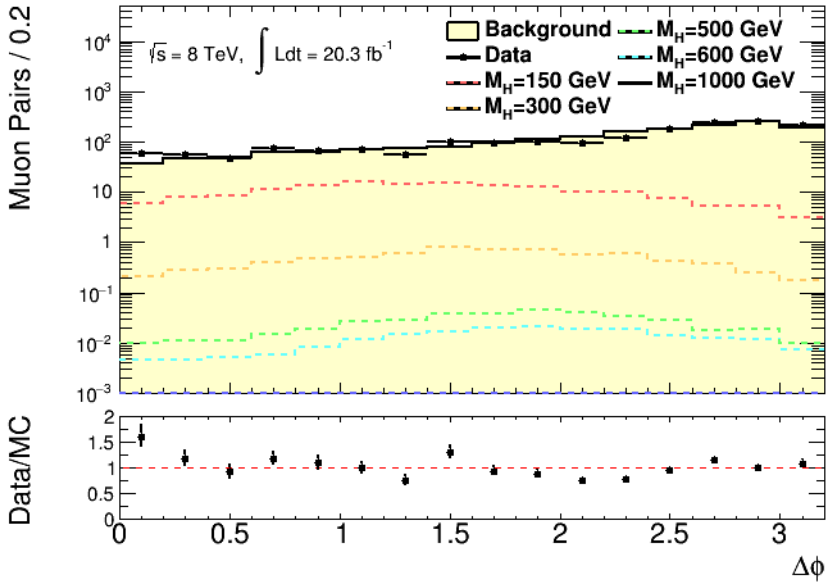

Figure 13: $\Delta\phi$ distribution for the total background, signal and data. The signals are represented as hatched lines, and the data are shown as closed circles with poisson errors.

Fig. 12 and Fig. 13 show positive result. As mentioned before, the MC samples were normalized to data instead of applying some corrections (see Sec. 5.1), and they show a very nice agreement with data and background for low p_{T} and m_{ll}. But it is not obvious that they should keep agreeing for higher p_{T} and m_{ll}, since the background MC samples were lacking statistics in these regions, but Fig. 12 indicates that the data and predicted background show a very nice agreement. With this in mind, one can conclude that no excess in data is observed, and this is not due to lack of background statistics or problems with the normalization, it simply means that no doubly-charged Higgs bosons were found. If data and background did not show a good agreement at higher p_{T} and m_{ll}, the validity of the optimization and the cuts could be questioned.

Five signal regions are examined in this analysis. The numerical result of the efficiency of the cuts are only discussed for three of these signal regions, namely for $m_H = 150\,\mathrm{GeV}$, $m_H = 500\,\mathrm{GeV}$, $m_H = 1000\,\mathrm{GeV}$. The results for the other regions are presented in Appendix A.6. The first region corresponds to a doubly-charged Higgs boson that is already excluded, but it has a high cross section that is valuable for testing the validity of the optimization. Table 3 presents the number of events passed for each type of background, signal and data, in the first column with no cuts applied, and the subsequent columns with the indicated cut implied in the first row. The errors presented are Gaussian. If no events pass the cuts, as is often the case when all of the cuts are applied to rare SM processes, an uncertainty is added corresponding to one event. Table 4 presents the same results, but with the relative efficiency of the cuts in percent.

$\mathbf{m_H = 150\,GeV}$	no cuts	Δm_H	p_T	$\Delta\phi$	$p_T + \Delta\phi$	All Cuts
WZ → lllν	1177.8±34.3	92.9±9.6	126.1±11.2	336.0±18.3	24.3±4.9	1.9±1.4
ZZ → llll	314.8±4.3	22.0±1.1	26.0±1.1	50.0±1.3	3.2±0.3	0.3±0.1
WW + 2j	6.5±0.1	0.6±0.0	1.3±0.1	2.3±0.1	0.4±0.0	0.0+1.0
$t\bar{t}$ + V	14.1±0.2	1.0±0.0	2.8±0.1	5.7±0.1	0.8±0.1	0.0+1.0
Fakes	300.0±3.7	7.9±0.4	6.8±0.3	84.5±2.0	1.7±0.2	0.3+0.1
Total Background	1813.2±42.6	124.4±11.2	163.0±12.8	478.6±21.9	30.4±5.5	2.5±1.6
MC $\mathbf{m_H = 150\,GeV}$	160.7±1.8	128.9±4.8	95.0±3.3	92.9±2.0	65.7±4.3	52.9±5.8
Data	1814	143	136	526	22	0

Table 3: The number of events obtained after applying the cuts determined by the optimization for $m_H = 150\,\text{GeV}$. The cuts are specified in Tab. 1. The errors indicated are Gaussian. The rows show the five dominant background processes, the total background, the signal MC and finally the real data. The V indicated in the fifth row of all tables is a boson, either W^+ or Z.

$\mathbf{m_H = 150\,GeV}$	Δm_H	p_T	$\Delta\phi$	$p_T + \Delta\phi$	All Cuts
WZ → lllν	7.9 %	10.7 %	28.5 %	2.1 %	0.2 %
ZZ → llll	7.0 %	8.3 %	15.9 %	1.0 %	0.1 %
WW + 2j	9.4 %	20.8 %	35.8 %	6.6 %	0.0 %
$t\bar{t}$ + V	7.0 %	20.0 %	40.6 %	5.5 %	0.2 %
Fakes	2.6 %	2.3 %	28.2 %	0.6 %	0.1 %
Total Background	6.9 %	9.0 %	26.4 %	1.7 %	0.1 %
MC $\mathbf{m_H = 150\,GeV}$	80.2 %	59.1 %	57.8 %	40.9 %	32.9 %
Data	7.9 %	7.5 %	29.0 %	1.2 %	0.0 %

Table 4: The efficiency of applying the cuts represented in percentage for $m_H = 150\,\text{GeV}$.

If a doubly-charged Higgs boson of mass $m_H = 150\,\text{GeV}$ existed, one would see 53 events passing the cuts. Obviously this is not the case since there are zero events in the data that passed the cuts. If it were the case, we would have had a detection with a significance of $33\,\sigma$. Since a doubly-charged Higgs boson of mass approximately $m_H < 450\,\text{GeV}$ has already been excluded, this was just a cross-check to see if these results were contradicting the results of previous analyses. The most interesting results in data are found in Tab 5, where one expects 1.7 ± 0.9 events passing the cuts if a doubly-charged Higgs boson of mass $m_H = 300\,\text{GeV}$ exists, and there is indeed 1 event passing the cuts in the data. Even though this could look like a detection of a doubly-charged Higgs boson, it should not be treated as one. First of all, it is contradicting established results of previous analyses that has excluded a doubly-charged Higgs of mass $m_H = 300\,\text{GeV}$. Secondly, the error included here are just statistical, and if the systematic uncertainties

were implemented, the errors would have been high enough that this would just look like a fluctuation, and not a detection.

$\mathbf{m_H = 300\,GeV}$	no cuts	Δm_H	p_T	$\Delta\phi$	$p_T + \Delta\phi$	All Cuts
$\mathbf{WZ \to lll\nu}$	1177.8±34.3	39.6±6.3	100.3±10.0	228.9±15.1	12.4±3.5	0.2+0.4
$\mathbf{ZZ \to llll}$	314.8±4.3	8.8±0.7	19.5±0.9	33.4±1.1	1.5±0.2	0.0+1.0
$\mathbf{WW + 2j}$	6.5±0.1	0.3±0.0	1.1±0.0	1.9±0.1	0.2±0.0	0.0+1.0
$\mathbf{t\bar{t} + V}$	14.1±0.2	0.5±0.0	2.3±0.1	4.1±0.1	0.4±0.1	0.0+1.0
Fakes	300.0±3.7	2.0±0.1	4.7±0.2	59.0±1.7	0.9±0.1	0.0+1.0
Total Background	1813.2±42.6	51.3±7.2	128.0±11.3	327.3±18.1	15.5±3.9	0.2+0.5
$\mathbf{MC\ m_H = 300\,GeV}$	7.4±0.1	6.1±0.4	7.0±0.3	2.2±0.1	2.1±0.3	1.7±0.9
Data	1814	45	114	370	16	1

Table 5: The effects of applying the cuts determined by the optimization for $m_H = 150\,\text{GeV}$. The cuts are specified in Tab. 1. The errors indicated are Gaussian. The V indicated in the 5th row of all tables is a boson, either $W^{\pm}$ or Z.

Tab. 6 and Tab. 7 present the same kind of results in percentage for $m_H = 500\,\text{GeV}$ and $m_H = 1000\,\text{GeV}$, but the number of events passed for each cut is presented in Appendix A.6. The Δm_H is obviously very efficient in keeping the signal, for all signal regions, which was predicted. For $m_H = 150\,\text{GeV}$ the $\Delta\phi$ and p_T are equally successful in keeping the signal, but the p_T cut is more efficient in reducing the background.

$\mathbf{m_H = 500\,GeV}$	Δm_H	p_T	$\Delta\phi$	$p_T + \Delta\phi$	All Cuts
$\mathbf{WZ \to lll\nu}$	0.8 %	8.5 %	26.1 %	1.5 %	0.0 %
$\mathbf{ZZ \to llll}$	0.7 %	6.2 %	14.2 %	0.6 %	0.0 %
$\mathbf{WW + 2j}$	1.9 %	17.0 %	34.9 %	4.7 %	0.0 %
$\mathbf{t\bar{t} + V}$	0.8 %	16.6 %	38.1 %	4.1 %	0.0 %
Fakes	0.0 %	1.6 %	25.6 %	0.3 %	0.0 %
Total Background	0.7 %	7.1 %	24.1 %	1.2 %	0.0 %
$\mathbf{MC\ m_H = 500\,GeV}$	82.0 %	99.4 %	35.5 %	35.3 %	28.0 %
Data	0.6 %	6.3 %	25.9 %	1.1 %	0.0 %

Table 6: The efficiency of applying the cuts represented in percentage for $m_H = 500\,\text{GeV}$.

$\mathbf{m_H = 1000\,GeV}$	Δm_H	p_T	$\Delta\phi$	$p_T + \Delta\phi$	All Cuts
$\mathbf{WZ \to lll\nu}$	0.1 %	17.9 %	62.0 %	8.3 %	0.0 %
$\mathbf{ZZ \to llll}$	0.0 %	14.1 %	45.8 %	4.1 %	0.0 %
$\mathbf{WW + 2j}$	0.0 %	29.2 %	68.9 %	17.0 %	0.0 %
$\mathbf{t\bar{t} + V}$	0.0 %	31.8 %	73.0 %	21.6 %	0.0 %
Fakes	0.0 %	5.1 %	58.1 %	3.5 %	0.0 %
Total Background	0.0 %	15.3 %	58.7 %	6.9 %	0.0 %
MC $\mathbf{m_H = 1000\,GeV}$	90.9 %	99.9 %	75.1 %	75.0 %	68.1 %
Data	0.1 %	13.7 %	55.7 %	6.0 %	0.0 %

Table 7: The efficiency of applying the cuts represented in percentage for $m_H = 1000\,\text{GeV}$.

As was predicted, the $\Delta\phi$ cut becomes less significant with higher doubly-charged Higgs masses, i.e. the increase in the $\Delta\phi$ cut allows to keep more of the signal, but it is at the same keeping a lot of background. One can conclude that as the $\Delta\phi$ cut becomes less important, the other cuts become more similar. This is due to the fact that the distributions of the signal and background become more distinguishable at higher mass regions, since the background invariant mass and muon p_T is centred in the low mass regions, whereas these distributions are centred in higher mass regions. Therefore, a low cut to reduce the background p_T is as efficient as keeping a high invariant peak of the signal. A common effect for all of the tables presented here, is that the cuts are equally efficient when applied to data and background. This gives a hint that the data is just composed of SM processes. The most dominant background processes are indeed the diboson processes ($W^+Z \to l^+\,\nu\,l^\pm\,l^\mp$, $W^-Z \to l^-\,\bar{\nu}\,l^\pm\,l^\mp$ and $ZZ \to l^-\,l^-\,l^+\,l^+$) but also the fake background in low p_T regions, therefore one can conclude that in order to properly estimate the background, it is essential to include fakes. The trends discussed for these mass points are also valid for the mass points presented in Appendix A.6.

The aim of this thesis has been to find variables that would help in isolating a potential doubly-charged Higgs boson, and to improve future searches for it. It would have been for nothing if these cuts did not improve the significance, so a last concluding measurement is done to see whether the cuts are actually valuable or not, by measuring the significance without any cuts applied. A previous search for a doubly-charged Higgs boson [13] has used the following cuts for the muon channel:

- Same-sign requirement.
- A Z veto excluding invariant mass pairs in the region $70 \leq m_{ll} \leq 110\,\text{GeV}$.
- A J/ψ veto excluding invariant mass pairs under $m_{ll} \leq 15\,\text{GeV}$.

The significances obtained by applying all, some and none of the cuts are presented in Tab. 8.

Cuts	$p_T + \Delta\phi + \Delta m_H$	$p_T + \Delta\phi$	Δm_H	No cuts
$\mathbf{m_H = 150\,GeV}$	33	12	12	4.2
$\mathbf{m_H = 300\,GeV}$	3.8	0.52	0.86	0.20
$\mathbf{m_H = 500\,GeV}$	1.7	0.030	0.091	0.011
$\mathbf{m_H = 600\,GeV}$	1.2	0.016	0.057	0.0054
$\mathbf{m_H = 1000\,GeV}$	0.044	0.0004	0.0054	0.0002

Table 8: The significances n_σ obtained by applying all, some and none of the cuts. "No cuts" are just the cuts presented in 5.4 (same-sign requirement, Z veto and J/ψ veto.).

The significances are indeed much improved by applying the cuts, but on should keep in mind that they never reach 3, let alone 5 which would imply a detection. Applying all of the three cuts provide a huge increase in significance. The more modest cuts on just p_T and $\Delta\phi$ provide at least a significance increased by a factor of two. The significance obtained when applying just the Δm_H cut is also presented in Tab. 8, and the significances obtained are approximately equal to those obtained for by applying the p_T and $\Delta\phi$ cuts.

6 Conclusions

To sum up all the results in this analysis is both encouraging and discouraging. The cuts obtained in this analysis show a drastic improvement of the significances, but no excess in data is observed. On these energy scales, the cross section for a production of doubly-charged Higgs bosons is very low and the amount of integrated luminosity required for a discovery is very large (see Appendix A.7 for a calculation of the required integrated luminosity) so this section will be spent on discussing how the future looks for doubly-charged Higgs bosons at higher cross sections and center-of-mass energies.

6.1 Optimized Cuts

The values presented in Tab. 1 follow the trends discussed in the previous section. The optimal value for the width Δm_H increases with the expected doubly-charged Higgs mass, reflecting the momentum and invariant mass resolution of the muon spectrometer. The $\Delta\phi$ cut follows the trend discussed regarding the boosted Higgs bosons, with an increasing value for higher Higgs masses. Unfortunately, this cut is the most effective for the lower mass regions, since the more boosted muons will allow to put a low upper cut on $\Delta\phi$, and thus excluding a big chunk of the background. An extrapolation of this effect will just lead to the $\Delta\phi$ cut becoming less and less significant for higher doubly-charged Higgs masses, as the $\Delta\phi$ of the signal and background distribution becomes more similar. That being said, it is still included in this analysis, because it is still providing a small reduction of the background in these signal regions, but as an outlook for Run II and higher energies in general, the $\Delta\phi$ will probably not be of interest. On a brighter note, there is not much of a fluctuation when it comes to the values of the p_T cut, which means it is assumed to be fairly

independent of the different signal regions. Therefore, the p_{T} cut can be treated as a more general cut, which is unbiased by the specific MC samples and the doubly-charged Higgs mass. A task in this analysis was to find variables to cut on that would be independent of the most obvious cut, the width Δm_H. The reason for this was that the invariant mass peaks are heavily correlated to the specific MC samples, and thus the mass of the Higgs. If one knew what the mass of the doubly-charged Higgs boson was, the most obvious cut would be around its mass peak. But since the mass of the doubly-charged Higgs boson is not known (yet), one should keep in mind that the cut on the width around the mass peak provides large significances that are biased to the specific MC samples. It is a common practice in analyses like this to generate signal MC samples for all of the possible masses (as opposed to only five mass points used in this analysis) for the doubly-charged Higgs boson or whichever particle one looks for. In that case, one can optimize signal regions for all of the masses, and the most efficient cut is then around the generated mass peaks corresponding to high significances. Then when unblinding the analysis, one can sweep over all the possible mass points, and if no excess is observed in data, one can exclude the existence of the particle at that mass. Therefore one can conclude that the cut around the mass peak is a very efficient cut and provides an efficient tool for finding or excluding particles, if more mass points are included. But for an analysis like this, with few mass points, other cuts should also be implemented. If the cut around the mass peak is included in future analyses, improvements could be made by take into account the binning around the peaks, which has not been implemented here. This could hopefully result in a better discrimination of the signal to background and thus provide more accurate cuts on the width.

Important results in this analysis are the significances obtained for applying the different sets of cuts. Applying all of the cuts results in a very high significance ($33\,\sigma$) for the lightest doubly-charged Higgs boson, and relatively high significance ($1.2\text{-}3.8\,\sigma$) for doubly-charged Higgs bosons of masses $m_H = 300\,\mathrm{GeV}$ to $m_H = 600\,\mathrm{GeV}$. This leads to the conclusion that these cuts are valid, but limited to searches for doubly-charged Higgs bosons of just five different masses. Just applying the p_{T} and $\Delta\phi$ cuts and just applying the Δm_H cut result in almost the same-significances, and thus one can conclude that the two sets of cuts are equally good, but the p_{T} and $\Delta\phi$ is more general since it is not depending less on the specific MC samples. To conclude, this analysis has found cuts that increase the significance by almost a factor of ten (compared to when no cuts are applied), which is a very drastic increase and should be seen as a success.

No excess in data is observed, but data and background show a very good agreement which is a good cross-check to secure the validity of this analysis.

Systematic uncertainties are not implemented in this analysis apart from when determining the non-prompt contribution, where the systematic uncertainty was almost 17% and to large to be neglected. When summing up the other systematic uncertainties they account for an uncertainty of approximately 5%.

6.2 Outlook

The main problem in this analysis has been to deal with the lack of statistics. Even though the whole Run I data set of $20.3\,\mathrm{fb}^{-1}$ has been used, the low cross sections for the production of doubly-charged Higgs bosons limits the validity of this optimization. One expects to find approximately one doubly-charged Higgs boson of mass $m_H = 1000\,\mathrm{GeV}$, ($N = \sigma \int L dt \implies 0.05\,\mathrm{fb} * 20.3\,\mathrm{fb}^{-1} \approx 1$). The low cross sections

make it really hard to isolate the signal, since it barely exists. But keeping in mind that these cross sections are generated for a specific center-of-mass energy ($\sqrt{s} = 8\,\text{TeV}$) and that they will increase[16] with the new center-of-mass energy of the LHC $\sqrt{s} = 14\,\text{TeV}$, this is increasing detection prospects. In the near future, the problem of lack of statistics will be accounted for during Run II, since the ATLAS detector is expected to generate an integrated luminosity of approximately $100\,\text{fb}^{-1}$. But until Run II, a way to deal with the lack of statistics in signal and background for high mass regions is to loosen the signal muon definition and allow for more fakes. The looser cuts in the muon selection would provide more statistics. The fake factors has an inherent high uncertainty related to it at higher p_{T} regions, which should be re-evaluated with more statistics during Run II. Systematic uncertainties should also be assessed in future analyses.

The aim of this analysis was not to find a doubly-charged Higgs boson, but rather possibly improve on the lower mass limits and provide insight on the efficiency of applying cuts in the search. In principle, the positive results on the significances found in this analysis could help in improving the mass limits that are already set on the doubly-charged Higgs bosons, by running a limit setting program.

The $\Delta\phi$ cut can be incorporated into future analyses, but just up to the point where the signal and background distribution becomes too similar, which happens for high enough Higgs masses, $m_H \geq 1000\,\text{GeV}$. The validity of the cut on the width around the mass peak Δm_H has been discussed in this thesis, and the conclusion to bring into future analyses is that it is an extremely efficient cut, but biased by an assumption on the mass of the doubly-charged Higgs. Future searches could generate signal MC samples for more mass points and use the Δm_{ll} cut for a search that thoroughly scans whole mass regions. Neural networks can be used to find correlations between cuts in the higher mass regions that are hard to optimize due to the low statistics. Results from this analysis on the efficiency of the cuts can be incorporated into future analyses, using higher center-of-mass energies, but also in general dilepton searches exploring final states with electron pairs, tauon pairs or lepton flavour violating pairs (such as electron-tauon or electron-muon pairs), or final states involving two same-sign lepton pairs.

All in all, the future for searches for doubly-charged Higgs bosons decaying into same-sign leptons looks bright and I am excited to see the results that the Run II will bring.

Acknowledgments

This thesis could not have been written without the help of Anders Floderus, the computer support of Florido Paganelli, the general ATLAS expertise of Lene Bryngemark and the support of Tuva Richert. A special thanks to Anthony Hawkins whose PhD thesis this analysis extends from and to Anders Oskarsson for proof reading. And finally I would like to thank my supervisor Else Lytken for the opportunity to work on this project.

[16] According to the collider reach tool [21].

A Appendix

A.1 Data Recorded

The data used in this analysis is all of the data recorded during Run I (period A-L) that is considered *Good*[17], at a center-of-mass energy of $\sqrt{s} = 8\,\text{TeV}$. The trigger used for the $\mu\mu$ channel is EF_mu18_tight_mu8_EFFS, a trigger that requires a leading muon with $p_\text{T} > 18\,\text{GeV}$ and a sub-leading muon with $p_\text{T} > 8\,\text{GeV}$.

A.2 Uncertainties

There are systematic uncertainties[18] entering into all stages of the analysis, such as the following, with the quoted errors found in [13]:

- Uncertainties associated with the MC statistics (3%).
- Uncertainties associated with muon reconstruction and identification (0.6%)
- Uncertainties associated with the efficiency of the triggers at different p_T and η of the muons (2.1-2.6%).
- Uncertainties in the integrated luminosity (2.8%).
- Uncertainties in the determination of the fake factor (17%).
- Uncertainties in the MC cross sections calculations (varies from process to process).

Worth mentioning is that the uncertainties treated in this analysis are just statistical, i.e. the systematic ones presented above are well known, but not taken into account, apart from the uncertainties in the determination of the fake factor which has a non-negligible systematic uncertainty of 17%.

A.3 Muon Selection

In Tab. 9, the selection requirements for muons are summarized. The muons should have a transverse momentum of more than 20 GeV. Pseudo-rapidity is defined as $\eta = -\ln(\tan(\theta/2))$ a spatial coordinate describing the angle of a particle relative to the beam axis where θ is the angle from the particle track to the beam axis. The impact parameter d_0 is the distance from the track to the collision point in the transverse direction. d_0 describes the proximity to the initial collision point, which ensures that the associated track comes from a point close enough to the collision point, i.e. the muon is prompt and not originating from for example a b-decay in flight. The requirement $Q_{ID} == Q_{MX}$ ensures that the charge measured in the ID is the same as the charge measured in the muon spectrometer. The jet overlap cut is to ensure that around a cone $\Delta R = \Delta\sqrt{(\Delta\eta)^2 + (\Delta\phi)^2}$, where $\Delta\eta$ and $\Delta\phi$ is the relative pseudo-rapidity and azimuthal angle ϕ between a jet and a muon to ensure that the muons are well isolated from the jets.

[17] Which means that the whole detector and the triggers were fully operational at the time of the recording.

[18] Which is an error that is introduced by an inaccuracy inherent in the system rather than an uncertainty determined by chance.

Selection	Muon requirement
Leading muon transverse momentum	$p_{\mathrm{T}} > 25\,\mathrm{GeV}$
Sub-leading muon transverse momentum	$p_{\mathrm{T}} > 20\,\mathrm{GeV}$
Muon pseudo-rapidity	$\lvert\eta\rvert < 2.5$
Impact Parameters	$\lvert d_0\rvert/\sigma(d_0) < 3$, $\lvert d_0\rvert < 0.2\,\mathrm{mm}$
Identification Criteria	ID hit requirements, $Q_{ID} == Q_{MX}$
Track Isolation	$\mathrm{ptcone30}/p_{\mathrm{T}} < 0.07$
Jet Overlap	$\Delta R(\mu, \mathrm{jet}) > 0.40$

Table 9: Table of signal muon definitions, taken from [13]

A.4 Cross Sections

The diboson SM background processes are generated with Sherpa 1.4.1 [17]. The other processes are generated with MADGRAPH-5.1.4.8 [18]. The cross sections for the different processes are presented in Tab. 10.

Process	Generator	Sample Number	Cross section (pb)
$WZ \to lll\nu$	SHERPA	126893	9.75
$ZZ \to llll$	SHERPA	126894	8.73
$WW + 2j$	MADGRAPH	158818	0.369
$t\bar{t} + W$	MADGRAPH	119353	0.104
$t\bar{t} + Z$	MADGRAPH	119355	0.068

Table 10: Monte Carlo samples used for the SM background processes

The cross sections for the doubly-charged Higgs processes generated with Pythia [19] are presented in Tab. 11.

Process	Generator	Cross section (fb)
$H^{\pm\pm} \to l^{\pm}l^{\pm}$, $m(H^{\pm\pm}) = 150\,\mathrm{GeV}$	Pythia	132
$H^{\pm\pm} \to l^{\pm}l^{\pm}$, $m(H^{\pm\pm}) = 300\,\mathrm{GeV}$	Pythia	8
$H^{\pm\pm} \to l^{\pm}l^{\pm}$, $m(H^{\pm\pm}) = 500\,\mathrm{GeV}$	Pythia	0.6
$H^{\pm\pm} \to l^{\pm}l^{\pm}$, $m(H^{\pm\pm}) = 600\,\mathrm{GeV}$	Pythia	0.2
$H^{\pm\pm} \to l^{\pm}l^{\pm}$, $m(H^{\pm\pm}) = 1000\,\mathrm{GeV}$	Pythia	0.05

Table 11: Monte Carlo samples used for the signal processes

A.5 Fake Factor Method

The fake factors used in this analysis are presented in Tab. 12, which in turn is obtained from [13]. The errors presented are the total errors, i.e. both systematic and statistical errors.

p_{T} Bin [GeV]	Fake Factor	Error [%]
(20,22)	0.125	16.8
(22, 25)	0.126	16.9
(25, 30)	0.113	17.3
(30, 35)	0.109	19.1
(35, 40)	0.131	22.7
(40, 60)	0.201	23.1
($>$ 60)	0.201	100

Table 12: Monte Carlo samples used for the signal processes

A.6 Additional Numerical Results

Tab. 13 to Tab. 17 present the additional numerical results obtained for the signal regions $m_H = 300\,\mathrm{GeV}$ and $m_H = 600\,\mathrm{GeV}$.

$\mathbf{m_H = 300\,GeV}$	Δm_H	p_T	$\Delta\phi$	$p_T + \Delta\phi$	All Cuts
$\mathbf{WZ \to lll\nu}$	3.4 %	8.5 %	19.4 %	1.1 %	0.0 %
$\mathbf{ZZ \to llll}$	2.8 %	6.2 %	10.6 %	0.5 %	0.0 %
$\mathbf{WW + 2j}$	4.7 %	17.0 %	29.2 %	3.8 %	0.0 %
$\mathbf{t\bar{t} + V}$	3.8 %	16.6 %	29.0 %	3.1 %	0.1 %
Fakes	0.7 %	1.6 %	19.7 %	0.3 %	0.0 %
Total Background	2.8 %	7.1 %	18.1 %	0.9 %	0.0 %
MC $\mathbf{m_H = 300\,GeV}$	82.7 %	94.0 %	29.6 %	27.7 %	22.8 %
Data	2.5 %	6.3 %	20.4 %	0.9 %	0.1 %

Table 13: The efficiency of applying the cuts represented in percentage for $m_H = 300\,\mathrm{GeV}$.

$\mathbf{m_H = 500\,GeV}$	no cuts	Δm_H	p_T	$\Delta\phi$	$p_T + \Delta\phi$	All Cuts
$\mathbf{WZ \to lll\nu}$	1177.8±34.3	9.9±3.1	100.3±10.0	308.0±17.5	17.8±4.2	0.0+1.0
$\mathbf{ZZ \to llll}$	314.8±4.3	2.3±0.3	19.5±0.9	44.8±1.2	1.9±0.2	0.0+1.0
$\mathbf{WW + 2j}$	6.5±0.1	0.1±0.0	1.1±0.0	2.3±0.1	0.3±0.0	0.0+1.0
$\mathbf{t\bar{t} + V}$	14.1±0.2	0.1±0.0	2.3±0.1	5.4±0.1	0.6±0.1	0.0+0.1
Fakes	300.0±3.7	0.1±0.0	4.7±0.2	76.9±1.9	0.9±0.1	0.0+1.0
Total Background	1813.2±42.6	12.5±3.5	128.0±11.3	437.3±20.9	21.5±4.6	0.0+0.1
MC $\mathbf{m_H = 500\,GeV}$	0.4±0.0	0.3±0.0	0.4±0.0	0.1±0.0	0.1±0.0	0.1+0.3
Data	1814	10	114	470	20	0

Table 14: The effects of applying the cuts determined by the optimization for $m_H = 500\,\text{GeV}$. The cuts are specified in Tab. 1. The errors indicated are Gaussian. The V indicated in the fifth row of all tables is a boson, either $W^{\pm}$ or Z.

$\mathbf{m_H = 600\,GeV}$	no cuts	Δm_H	p_T	$\Delta\phi$	$p_T + \Delta\phi$	All Cuts
$\mathbf{WZ \to lll\nu}$	1177.8±34.3	7.1±2.7	100.3±10.0	371.4±19.3	22.4±4.7	0.0+1.0
$\mathbf{ZZ \to llll}$	314.8±4.3	1.3±0.2	19.5±0.9	55.9±1.4	2.0±0.2	0.0+1.0
$\mathbf{WW + 2j}$	6.5±0.1	0.1±0.0	1.1±0.0	2.4±0.1	0.3±0.0	0.0+1.0
$\mathbf{t\bar{t} + V}$	14.1±0.2	0.1±0.0	2.3±0.1	6.2±0.2	0.7±0.1	0.0+0.1
Fakes	300.0±3.7	0.0±1.0	4.7±0.2	91.5±2.1	1.1±0.1	0.0+1.0
Total Background	1813.2±42.6	8.6±2.9	128.0±11.3	527.5±23.0	26.5±5.1	0.0+0.1
$\mathbf{MC\ m_H = 600\,GeV}$	0.2±0.0	0.2±0.0	0.2±0.0	0.1±0.0	0.1±0.0	0.1+0.2
Data	1814	6	114	572	24	0

Table 15: The effects of applying the cuts determined by the optimization for $m_H = 600\,\text{GeV}$. The cuts are specified in Tab. 1. The errors indicated are Gaussian. The V indicated in the fifth row of all tables is a boson, either $W^{\pm}$ or Z.

$\mathbf{m_H = 600\,GeV}$	Δm_H	p_T	$\Delta\phi$	$p_T + \Delta\phi$	All Cuts
$\mathbf{WZ \to lll\nu}$	0.6 %	8.5 %	31.5 %	1.9 %	0.0 %
$\mathbf{ZZ \to llll}$	0.4 %	6.2 %	17.8 %	0.6 %	0.0 %
$\mathbf{WW + 2j}$	1.9 %	17.0 %	37.7 %	4.7 %	0.0 %
$\mathbf{t\bar{t} + V}$	0.7 %	16.6 %	44.3 %	4.9 %	0.0 %
Fakes	0.0 %	1.6 %	30.5 %	0.4 %	0.0 %
Total Background	0.5 %	7.1 %	29.1 %	1.5 %	0.0 %
$\mathbf{MC\ m_H = 600\,GeV}$	85.0 %	99.5 %	41.3 %	41.2 %	34.5 %
Data	0.3 %	6.3 %	31.5 %	1.3 %	0.0 %

Table 16: The efficiency of applying the cuts represented in percentage for $m_H = 600\,\text{GeV}$.

$\mathbf{m_H = 1000\,GeV}$	no cuts	Δm_H	p_T	$\Delta\phi$	$p_T + \Delta\phi$	All Cuts
$\mathbf{WZ \to lll\nu}$	1177.8±34.3	0.7±0.8	211.2±14.5	730.7±27.0	97.4±9.9	0.0+1.0
$\mathbf{ZZ \to llll}$	314.8±4.3	0.1±0.1	44.4±1.5	144.0±2.5	12.9±0.6	0.0+1.0
$\mathbf{WW + 2j}$	6.5±0.1	0.0±1.0	1.9±0.1	4.4±0.1	1.1±0.1	0.0+1.0
$\mathbf{t\bar{t} + V}$	14.1±0.2	0.0±0.0	4.5±0.1	10.3±0.2	3.0±0.1	0.0+1.0
Fakes	300.0±3.7	0.0±1.0	15.3±0.5	174.3±2.8	10.5±0.5	0.0+1.0
Total Background	1813.2±42.6	0.8±0.9	277.3±16.7	1063.7±32.6	124.9±11.2	0.0+1.0
$\mathbf{MC\ m_H = 1000\,GeV}$	0.0±0.0	0.0±0.0	0.0±0.0	0.0±0.0	0.0±0.0	0.0+0.1
Data	1814	2	248	1011	108	0

Table 17: The effects of applying the cuts determined by the optimization for $m_H = 1000\,\text{GeV}$. The cuts are specified in Tab. 1. The errors indicated are Gaussian.

A.7 Integrated Luminosity Caluclations

To calculate the amount of integrated luminosity needed for a discovery of a particle, one can use Eq. A.7:

$$N = \sigma \int_0^\tau L dt \tag{23}$$

which is related to Eq. 21:

$$n_\sigma = \sqrt{L_{int}} \frac{\sigma_S}{\sqrt{\sigma_B}}. \tag{24}$$

A discovery is assumed to have been made when $n_\sigma \geq 5$. A back of the envelope calculation can be performed to get a feel of how much integrated luminosity is required for a discovery. Using the cross section for the most dominant SM background ($WZ \to lll\nu$) $\sigma_B = 9750\,\text{fb}$ and the cross section for the production of the lightest doubly-charged Higgs boson ($m_H = 150\,\text{GeV}$) $\sigma_S = 132\,\text{fb}$. For these values, the integrated luminosity needed for a detection is approximately $L_{int} \geq 14\,\text{fb}^{-1}$. Since the cross section for the doubly-charged Higgs bosons heavily decreases with mass (see Tab. 11), the integrated luminosity required for a detection for $m_H = 300\,\text{GeV}$ is much higher, namely $L_{int} \geq 3809\,\text{fb}^{-1}$. This provides a feel for the amount of data needed for a discovery at these energy scales.

References

[1] Kane, Gordon: *Modern Elementary Particle Physics.* Addison-Wesley, Massachusetts. 1993.

[2] M. E. Peskin, D. V. Schroeder, *An Introduction to Quantum Field Theory*, Ed. Westview, Boulder 1995.

[3] Y. Fukuda *et al.* [Super-Kamiokande Collaboration], Phys. Rev. Lett. **81** (1998) 1158 [Phys. Rev. Lett. **81** (1998) 4279] [hep-ex/9805021].

[4] K. Huitu and J. Maalampi, Phys. Lett. B **344** (1995) 217 [hep-ph/9410342].

[5] A. G. Akeroyd and M. Aoki, Phys. Rev. D **72** (2005) 035011 [hep-ph/0506176].

[6] "Cern Website" www.cern.ch.

[7] [ATLAS Collaboration], CERN-LHCC-97-16, ATLAS-TDR-4.

[8] [ATLAS Collaboration], CERN-LHCC-96-40.

[9] [ATLAS Collaboration], CERN-LHCC-97-22, ATLAS-TDR-10.

[10] G. Aad *et al.* [ATLAS Collaboration], Eur. Phys. J. C **74** (2014) 9, 3034 [arXiv:1404.4562 [hep-ex]].

[11] S. Chatrchyan *et al.* [CMS Collaboration], Eur. Phys. J. C **72** (2012) 2189 [arXiv:1207.2666 [hep-ex]].

[12] G. Aad *et al.* [ATLAS Collaboration], Eur. Phys. J. C **72** (2012) 2244 [arXiv:1210.5070 [hep-ex]].

[13] A.Hawkins. Search for beyond Standard Model physics with same-sign dileptons. PhD Thesis, U. Lund, Lund, 2014. http://lup.lub.lu.se/record/4738896

[14] G. Aad *et al.* [ATLAS Collaboration], arXiv:1411.2921 [hep-ex].

[15] W. Herr, B. J. Holzer, B. Muratori; *Concept of Luminosity* Landolt-Börnstein - Group I Elementary Particles, Nuclei and Atoms, 2013.

[16] W-M Yao et al 2006 J. Phys. G: Nucl. Part. Phys. 33 1

[17] T. Gleisberg, S. Hoeche, F. Krauss, M. Schonherr, S. Schumann, F. Siegert and J. Winter, JHEP **0902** (2009) 007 [arXiv:0811.4622 [hep-ph]].

[18] J. Alwall, P. Demin, S. de Visscher, R. Frederix, M. Herquet, F. Maltoni, T. Plehn and D. L. Rainwater *et al.*, JHEP **0709** (2007) 028 [arXiv:0706.2334 [hep-ph]].

[19] T. Sjostrand, S. Mrenna and P. Z. Skands, Comput. Phys. Commun. **178** (2008) 852 [arXiv:0710.3820 [hep-ph]].

[20] R. Brun and F. Rademakers, ROOT - An Object Oriented Data Analysis Framework, Proceedings AIHENP'96 Workshop, Lausanne, Sep. 1996, Nucl. Inst. & Meth. in Phys. Res. A 389 (1997) 81-86. See also http://root.cern.ch/.

[21] http:collider-reach.web.cern.ch